Noninstantaneous approximation to the Bethe-Salpeter equation

R. S. Bhalerao* and S. A. Gurvitz
Physics Department, Weizmann Institute of Science, Rehovot, Israel
(Received 10 December 1982)

A new relativistic three-dimensional two-body equation is presented. If the negative energy poles of the two-body propagator are neglected, this equation is exactly equivalent to the Bethe-Salpeter equation. In the derivation of this equation from the Bethe-Salpeter equation, retardation effects in the two-body interaction are treated carefully by taking fully into account contributions of the exchanged-"meson" singularities. The results are presented for the two cases: (a) the driving term in the Bethe-Salpeter equation is given by the relativistic one-meson exchange diagram (the ladder approximation) and (b) the driving term also includes relativistic crossed diagrams. Using these results it is shown that the Bethe-Salpeter equation in the ladder approximation goes over to the Lippmann-Schwinger equation in the nonrelativistic limit. But unlike the Blankenbecler-Sugar and Gross equations, the two-body potential is *not* the nonrelativistic Yukawa potential. It is given by an infinite sum of terms corresponding to instantaneous multimeson exchange contributions in the nonrelativistic two-body interaction. A method is presented which in the low energy limit greatly simplifies the calculation with crossed diagrams. The theory is applied to the problem of two scalar "nucleons" exchanging scalar "mesons," and comparisons are made with other relativistic equations. Also a simple model calculation is performed to demonstrate the sensitivity of phenomenological meson masses and meson-nucleon coupling constants to the theoretical reduction scheme chosen.

[NUCLEAR STRUCTURE Three-dimensional reduction of the Bethe-Salpeter equation. Ladder approximation. Crossed diagrams. Nonrelativistic limit. Instantaneous multimeson exchange.]

I. INTRODUCTION

In nonrelativistic quantum mechanics the problem of two-nucleon scattering is described by the Lippmann-Schwinger equation

$$T_{NN}(E,\vec{P},\vec{Q},\vec{Q}')=V_{NN}(\vec{Q},\vec{Q}')+\int \frac{V_{NN}(\vec{Q},\vec{Q}'')T_{NN}(E,\vec{P},\vec{Q}'',\vec{Q}')}{E-\frac{\vec{Q}''^2}{2m}-\frac{(\vec{P}-\vec{Q}'')^2}{2m}+i\epsilon}\frac{d^3Q''}{(2\pi)^3(2m)^2}\ , \tag{1.1}$$

which is shown schematically in Fig. 1. If the potential V_{NN} is generated by the exchange of a single meson then

$$V_{NN}(\vec{Q},\vec{Q}')=-\frac{g^2}{(\vec{Q}-\vec{Q}')^2+\mu^2}\ , \tag{1.2}$$

which is the well-known Yukawa potential. In Eqs. (1.1) and (1.2), $\vec{Q}$ and $\vec{Q}'$ are the initial and final three-momenta of one of the nucleons, μ is the mass of the exchanged virtual meson, g is meson-nucleon coupling constant, and m is the nucleon mass. $\vec{P}$ and E in Eq. (1.1) are the total momentum and kinetic energy of the two-nucleon system. E can be on or off the mass shell. [The on-shell value of E corresponds to $E=\vec{Q}^2/2m+(\vec{P}-\vec{Q})^2/2m=\vec{Q}'^2/2m+(\vec{P}-\vec{Q}')^2/2m$.] For the sake of simplicity we consider the nucleons and mesons as scalar particles.

For the relativistic generalization of the Lippmann-Schwinger equation we should introduce explicitly in Eq. (1.1) the energy of each virtual nucleon. We therefore rewrite *identically* the Lippmann-Schwinger equation (1.1) in the form

$$T_{NN}(E,\vec{P},\vec{Q},\vec{Q}')=V_{NN}(\vec{Q},\vec{Q}')+i\int\frac{V_{NN}(\vec{Q},\vec{Q}'')T_{NN}(E,\vec{P},\vec{Q}'',\vec{Q}')d^3Q''dQ_0''(2\pi)^{-4}}{\left[Q_0''-m-\frac{\vec{Q}''^2}{2m}+i\epsilon\right]\left[P_0-Q_0''-m-\frac{(\vec{P}-\vec{Q}'')^2}{2m}+i\epsilon\right](2m)^2}\ , \tag{1.3}$$

where Q_0'' is the energy of a virtual nucleon, P_0 is the total energy of the system ($P_0=E+2m$), and therefore P_0-Q_0'' is the energy of the second virtual nucleon. The relativistic generalization of the Lippmann-Schwinger equation, written in the form (1.3), is now straightforward: We have to replace the nonrelativistic two-nucleon propagator in Eq. (1.3) by the relativistic invariant propagator

$$\{[Q_0''^2-\vec{Q}''^2-m^2+i\epsilon][(P_0-Q_0'')^2-(\vec{P}-\vec{Q}'')^2-m^2+i\epsilon]\}^{-1}\ .$$

The new element which is introduced because of this replacement is the negative energy nucleon poles in the relativistic two-nucleon propagator, which do not exist in the nonrelativistic Lippmann-Schwinger equation (1.1) or (1.3). These poles correspond to the virtual nucleon pair production (the pair current effect). [If we neglect their contribution and perform dQ_0'' integration taking into account the positive energy nucleon poles only, we arrive at a three-dimensional equation which coincides in the nonrelativistic limit with the Lippmann-Schwinger equation (1.1).] For a relativistic generalization of Eq. (1.3) it is also necessary to replace the nonrelativistic Yukawa potential in Eq. (1.2) by the relativistic invariant Yukawa potential:

$$V_{NN}(Q,Q')=\frac{g^2}{(Q_0-Q_0')^2-(\vec{Q}-\vec{Q}')^2-\mu^2+i\epsilon}\ , \tag{1.4}$$

where $Q=(Q_0,\vec{Q})$ and $Q'=(Q_0',\vec{Q}')$ are the initial and final four-momenta of one of the nucleons. Thus we obtain the following relativistic equation for the two-nucleon scattering amplitude:

$$T_{NN}(P,Q,Q')=V_{NN}(Q,Q')+i\int\frac{V_{NN}(Q,Q'')T_{NN}(P,Q'',Q')d^4Q''}{[Q''^2-m^2+i\epsilon][(P-Q'')^2-m^2+i\epsilon](2\pi)^4}\ . \tag{1.5}$$

This is the well-known Bethe-Salpeter equation[1] (in the ladder approximation) obtained here as a straightforward generalization of the nonrelativistic Lippmann-Schwinger equation.[2] It too can be represented as in Fig. 1, with $\vec{P}$, $\vec{Q}$, and $\vec{Q}'$ replaced by four-momenta P, Q, and Q', respectively.

We ask ourselves the following question: What is the nonrelativistic limit[3] ($v/c\ll 1$) of the Bethe-Salpeter equation, Eq. (1.5), in the ladder approximation? A simple-minded answer would be the Lippmann-Schwinger equation with the nonrelativistic Yukawa potential, Eqs. (1.1) and (1.2). However, as the following physical argument shows, this answer is not correct. The reason is that the interaction described by the relativistic Yukawa potential Eq. (1.4) is not instantaneous. Because of retardation, the Bethe-Salpeter equation allows the processes where two or more mesons are "in the air" at the same time. The nonrelativistic interaction, on the other hand, is instantaneous. In this limit the processes where two or more mesons are present in an intermediate state at the same time do not vanish. They merely go over to the instantaneous exchanges of two or more mesons at the same time. Thus in the nonrelativistic limit the Bethe-Salpeter equation goes over to the Lippmann-Schwinger equation, but with a modified NN potential. This potential contains, together with the usual Yukawa potential corresponding to the one-meson exchange, Eq. (1.2), also terms corresponding to simultaneous exchanges of two or more mesons.

In order to derive the nonrelativistic limit of the Bethe-Salpeter equation it is necessary to perform a three-dimensional reduction of this equation, which amounts to performing the Q_0'' integration in Eq. (1.5). In most of the standard approaches found in the literature and often used in relativistic two-body calculations, it is done in an approximate way by replacing the four-dimensional propagator in the Bethe-Salpeter equation (1.5) by a three-dimensional one. The physical condition which is required to be fulfilled is that the approximate propagator should generate the same elastic unitarity cut as the exact

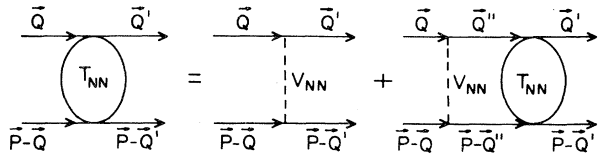

FIG. 1. Schematic representation of the Lippmann-Schwinger equation.

propagator. This condition does not uniquely define the approximate propagator.[4] Therefore many different approximate three-dimensional equations have been proposed.[5] However, the above procedure neglects the singularities of the integrand in Eq. (1.5) associated with the production of mesons in the intermediate states. This is an undesirable procedure since these singularities are intimately connected with the multimeson exchange processes mentioned earlier. It is thus not surprising that in the nonrelativistic limit these equations[5] go over to the Lippmann-Schwinger equation with the nonrelativistic Yukawa potential (1.2). The additional contributions from the instantaneous multimeson exchange do not appear. In order to retain these terms one should use a different procedure for three-dimensional reduction of the Bethe-Salpeter equation which takes into account meson production singularities.

We encountered the problem of three-dimensional reduction of the Bethe-Salpeter equation in Refs. 6 and 7 where we studied relativistic effects in deuteron form factors. Although our main aim there was to perform a three-dimensional reduction of the (ladder approximated) Bethe-Salpeter equation in order to obtain a deuteron wave function in a moving frame, we also had to perform the reduction in the case of the two-nucleon scattering amplitude, Eqs. (1.4) and (1.5). This reduction was done without neglecting the meson production singularities of the integrand in Eq. (1.5). Singularities associated with the virtual nucleon pair production being farther from the physical region were neglected, and calculations were made assuming scalar nucleons and bosons. The resulting three-dimensional equation[7] was of the Lippmann-Schwinger type with the effective potential in the form of an infinite series. Successive terms of this series contained an increasing number of intermediate mesons present at the same time. In the nonrelativistic limit the first term of this series reduces to the Yukawa potential, Eq. (1.2), the second term to an instantaneous exchange of two mesons, and so on, in accordance with the physical argument given above.

In this paper we concentrate on the detailed analysis of our approach and compare its predictions with those of the Bethe-Salpeter equation and other three-dimensional approximations to the Bethe-Salpeter equation. Since we pay special attention to the correct treatment of the retardation in the NN interaction we call our equation a "noninstantaneous approximation" to the Bethe-Salpeter equation. (Our equation is not fully equivalent to the Bethe-Salpeter equation, since we disregarded nucleon pair production singularities in our three-dimensional reduction.)

In this paper we also generalize our approach to include any general crossed diagram in the driving term of the Bethe-Salpeter equation, thus going beyond the ladder approximation. In the low energy limit the general result has a simple form. It can therefore be very useful for practical calculations of the Bethe-Salpeter equation, and may open a new way for an approximate treatment of multimeson exchange contributions in the NN potential.

The plan of the paper is as follows. In Sec. II we describe our three-dimensional reduction scheme for the Bethe-Salpeter equation in the ladder approximation. The numerical results are presented and discussed in Sec. III. In this section we also describe a simple model calculation which shows the sensitivity of the phenomenological meson masses and meson-nucleon coupling constants to the theoretical reduction scheme chosen. The derivation in Sec. II is generalized in Sec. IV to incorporate crossed diagrams. The corresponding numerical results and nonrelativistic limit are also presented and discussed in this section. In the last section we discuss some of our results in connection with the works of other authors.

II. THREE-DIMENSIONAL REDUCTION OF THE BETHE-SALPETER EQUATION

Consider again the Bethe-Salpeter equation for the two-body scattering amplitude

$$T = V + VGT \ , \tag{2.1}$$

where G is the relativistic two-body propagator as in Eq. (1.5) and V is the sum of all connected two-particle irreducible diagrams. In the ladder approximation V is given by Eq. (1.4). A commonly used scheme for three-dimensional reduction of the Bethe-Salpeter equation consists in replacing G by $g+(G-g)$, where g is a three-dimensional two-body propagator generating the same elastic unitarity cut. This leads to the following two coupled equations:

$$T = W + WgT \ , \tag{2.2}$$

$$W = V + V(G-g)W \ . \tag{2.3}$$

Iterating Eq. (2.3) one obtains

$$W = V + V(G-g)V + V(G-g)V(G-g)V + \cdots \ . \tag{2.4}$$

Equations (2.2) and (2.3) as they stand are exactly equivalent to the Bethe-Salpeter equation (2.1). However, solving these equations is as complicated as solving the original Eq. (2.1). Hence what is often done is to replace W in Eq. (2.2) by V. It is known that infinitely many different g's exist, all leading to three-dimensional equations satisfying

relativistic elastic unitarity.[4] [Thus it is desirable to have a g which makes the series in Eq. (2.4) converge rapidly making $W=V$ a good approximation. Unfortunately it is hard to follow this procedure since the calculation of second and higher order terms of Eq. (2.4) is difficult.] Here we consider the two most widely used choices of g, namely those of Blankenbecler-Sugar[5] and Gross.[5,8] We will work in the center of mass frame ($\vec{P}=0$ in Fig. 1). The Blankenbecler-Sugar equation corresponds to

$$g=\frac{\pi i\delta\left[Q_0''-\frac{P_0}{2}\right]}{2E_{\vec{Q}''}(E_{\vec{Q}''}{}^2-\frac{1}{4}P_0{}^2-i\epsilon)}\ , \tag{2.5}$$

where

$$E_{\vec{Q}''}=(m^2+\vec{Q}''^2)^{1/2}$$

and P_0 is the total energy of the system. In the center-of-mass frame the on-shell value of P_0 is

$$P_0=2(m^2+\vec{Q}^2)^{1/2}=2(m^2+\vec{Q}'^2)^{1/2}\ .$$

We can see that this choice of g corresponds to taking the intermediate nucleons on shell or equally off the mass shell; the virtual mass of each of the nucleons is the same:

$$(P_0{}^2/4-\vec{Q}''^2)^{1/2}\ .$$

The Gross equation corresponds to a different choice of g, namely

$$g=\frac{\pi i\delta(Q_0''-E_{\vec{Q}''})}{2E_{\vec{Q}''}P_0(E_{\vec{Q}''}-\frac{1}{2}P_0-i\epsilon)}\ . \tag{2.6}$$

One can see that this choice corresponds to taking one of the nucleons on the mass shell (for example, the nucleon with momentum $\vec{Q}''$ in Fig. 1).

In order to form three-dimensional equations, one should use the same procedure also for the external nucleons. This means that in the case of the Blankenbecler-Sugar equation the external nucleons are also on shell or equally off the mass shell: $Q_0=Q_0'=P_0/2$. In the Gross equation, on the other hand, the nucleon which is taken on the mass shell in the intermediate state is taken on the mass shell also in the initial and final states: $Q_0=E_{\vec{Q}}$ and $Q_0'=E_{\vec{Q}'}$.

Applying these procedures to the Bethe-Salpeter equation in the ladder approximation, Eqs. (1.4) and (1.5), we find in the center-of-mass frame the Blankenbecler-Sugar equation:

$$T_{NN}(P_0,\vec{Q},\vec{Q}')=\frac{-g^2}{(\vec{Q}-\vec{Q}')^2+\mu^2}+\int\frac{-g^2}{(\vec{Q}-\vec{Q}'')^2+\mu^2}\frac{T_{NN}(P_0,\vec{Q}'',\vec{Q}')}{E_{\vec{Q}''}(P_0{}^2/4-E_{\vec{Q}''}{}^2+i\epsilon)}\frac{d^3Q''}{32\pi^3}\ , \tag{2.7}$$

and the Gross equation:

$$T_{NN}(P_0,\vec{Q},\vec{Q}')=\frac{-g^2}{(\vec{Q}-\vec{Q}')^2-(E_{\vec{Q}}-E_{\vec{Q}'})^2+\mu^2}+\int\frac{-g^2}{(\vec{Q}-\vec{Q}'')^2-(E_{\vec{Q}}-E_{\vec{Q}''})^2+\mu^2}\frac{T_{NN}(P_0,\vec{Q}'',\vec{Q}')}{E_{\vec{Q}''}P_0(P_0/2-E_{\vec{Q}''}+i\epsilon)}\frac{d^3Q''}{32\pi^3}\ . \tag{2.8}$$

Although these equations are different, in the nonrelativistic limit they both go over to the usual Lippmann-Schwinger equation (1.1) with the nonrelativistic Yukawa potential (1.2). This limit corresponds to the following replacements in Eqs. (2.7) and (2.8):

$$\begin{aligned}&E_{\vec{Q}''}\left[\frac{P_0{}^2}{4}-E_{\vec{Q}''}{}^2\right]\to m^2\left[E-\frac{\vec{Q}''^2}{m}\right],\\ &E_{\vec{Q}''}P_0\left[\frac{P_0}{2}-E_{\vec{Q}''}\right]\to m^2\left[E-\frac{\vec{Q}''^2}{m}\right],\\ &(\vec{Q}-\vec{Q}')^2+\mu^2\gg(E_{\vec{Q}}-E_{\vec{Q}'})^2\ ,\end{aligned} \tag{2.9}$$

where $P_0=E+2m$, and $2m\gg E$.

However, as shown in Sec. I, a three-dimensional reduction of the Bethe-Salpeter equation should in the nonrelativistic limit give rise to terms in the NN potential which correspond to the multimeson exchange processes discussed earlier. These terms are clearly absent if one uses the Blankenbecler-Sugar or Gross procedures for three-dimensional reduction of the Bethe-Salpeter equation. Of course these terms would be taken into account if one includes higher order terms in W in Eq. (2.4). However, these terms include four-dimensional integrals, and their treatment is not easy. Moreover, since they involve two-nucleon (without mesons) intermediate states, they

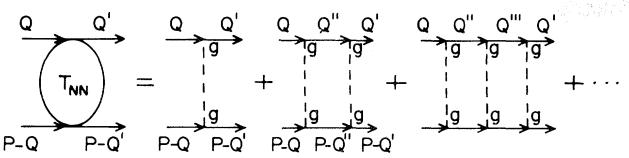

FIG. 2. Born series for the Bethe-Salpeter amplitude T_{NN}.

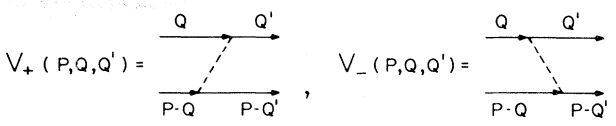

FIG. 3. Relativistic Yukawa potential $V_{NN}=V_{+}+V_{-}$.

are different from what one usually calls the multimeson exchange contribution to the potential, and their physical interpretation is not simple.

In Ref. 7 we derived an alternative procedure for three-dimensional reduction of the Bethe-Salpeter equation. Unlike the Blankenbecler-Sugar and Gross methods, this procedure does not involve construction of an approximate three-dimensional propagator g. We rather performed the Q_0'' integration in Eq. (1.5) without neglecting the boson singularities of the integrand. The only approximation in this otherwise exact procedure is that the negative energy nucleon poles of the propagator were not taken into account. In the following we will always work in the center of mass frame ($\vec{P}=0$). Thus

$$\begin{aligned}[Q''^2-m^2+i\epsilon][(P-Q'')^2-m^2+i\epsilon]&\\ \equiv(Q_0''-E_{\vec{Q}''}+i\epsilon)(P_0-Q_0''-E_{\vec{Q}''}+i\epsilon)&\\ \times(Q_0''+E_{\vec{Q}''}-i\epsilon)(P_0-Q_0''+E_{\vec{Q}''}-i\epsilon)&\\ \cong(Q_0''-E_{\vec{Q}''}+i\epsilon)(P_0-Q_0''-E_{\vec{Q}''}+i\epsilon)2E_{\vec{Q}''}P_0\ .&\end{aligned} \tag{2.10}$$

In Eq. (2.10) we approximated the product of the negative energy nucleon propagators

$$(Q_0''+E_{\vec{Q}''})(P_0-Q_0''+E_{\vec{Q}''})$$

by $2E_{\vec{Q}''}P_0$, assuming that the main contribution to the Q_0'' integral comes from the positive energy nucleon poles $Q_0''=E_{\vec{Q}''}$ and $Q_0''=P_0-E_{\vec{Q}''}$. It is straightforward to show that if, in the Bethe-Salpeter equation (1.5) one neglects the Q_0'' dependence of V_{NN} and T_{NN} and performs the Q_0'' integration in the approximation (2.10), one gets the Gross equation (2.8). On the other hand, if one neglects the Q_0'' dependence of V_{NN} and T_{NN} but does not make the approximation (2.10), one gets the Blankenbecler-Sugar equation (2.7).

Now we perform the three-dimensional reduction of Eq. (1.5) by treating the boson singularities in the integrand exactly. We first consider the Bethe-Salpeter equation in the ladder approximation. In this way we will obtain the result in Ref. 7, though in a more straightforward manner. Afterwards, we will allow any general crossed diagram in the driving term of the Bethe-Salpeter equation.

The easiest way to carry out Q_0'' integration in the Bethe-Salpeter equation (1.5) is to expand the right-hand side of this equation as an infinite Born series, and then perform the integration in each term separately. Iterating Eq. (1.5) we obtain the Born series for the amplitude T_{NN}, Fig. 2. We also rewrite the relativistic Yukawa potential as a sum of two "time-ordered" terms: $V_{NN}=V_{+}+V_{-}$, Fig. 3, where

$$\begin{aligned}V_{+}(P,Q,Q')&=\frac{g^2}{2\omega_{\vec{Q}-\vec{Q}'}(Q_0'-Q_0-\omega_{\vec{Q}-\vec{Q}'}+i\epsilon)}\ ,\\ V_{-}(P,Q,Q')&=\frac{g^2}{2\omega_{\vec{Q}-\vec{Q}'}(Q_0-Q_0'-\omega_{\vec{Q}-\vec{Q}'}+i\epsilon)}\ ,\end{aligned} \tag{2.11}$$

and $\omega_{\vec{Q}-\vec{Q}'}=[\mu^2+(\vec{Q}-\vec{Q}')^2]^{1/2}$.

Consider now the second Born term VGV in Fig. 2. It can be rewritten as a sum of four terms

$$\begin{aligned}T_{NN}^{(2)}=&V_{+}GV_{+}+V_{+}GV_{-}\\ &+V_{-}GV_{+}+V_{-}GV_{-}\ .\end{aligned} \tag{2.12}$$

Making use of the approximation (2.10) for the two-nucleon propagator, the first contribution $V_{+}GV_{+}$ is

$$V_{+}GV_{+}=ig^4\int\frac{(8P_0E_{\vec{Q}''}\omega_{\vec{Q}-\vec{Q}''}\omega_{\vec{Q}''-\vec{Q}'})^{-1}(2\pi)^{-4}dQ_0''d^3Q''}{(P_0-Q_0''-E_{\vec{Q}''}+i\epsilon)(Q_0''-E_{\vec{Q}''}+i\epsilon)(Q_0''-Q_0-\omega_{\vec{Q}''-\vec{Q}}+i\epsilon)(Q_0'-Q_0''-\omega_{\vec{Q}''-\vec{Q}'}+i\epsilon)}\ . \tag{2.13}$$

Integrating over the Q_0'' variable we get, after some algebra,

$$V_+GV_+ = g^4 \int \frac{(8P_0 E_{\vec{Q}''}\omega_{\vec{Q}-\vec{Q}''}\omega_{\vec{Q}''-\vec{Q}'})^{-1}}{P_0 - Q_0 - \omega_{\vec{Q}''-\vec{Q}} - E_{\vec{Q}''} + i\epsilon} \left[\frac{1}{P_0 - 2E_{\vec{Q}''} + i\epsilon} + \frac{1}{Q_0' - Q_0 - \omega_{\vec{Q}''-\vec{Q}} - \omega_{\vec{Q}'-\vec{Q}''} + i\epsilon} \right] \times \frac{(2\pi)^{-3} d^3Q''}{Q_0' - E_{\vec{Q}''} - \omega_{\vec{Q}'-\vec{Q}''} + i\epsilon} . \tag{2.14}$$

The two terms in Eq. (2.14) correspond to the two time-ordered diagrams of the old-fashioned perturbation theory and can be represented as in Fig. 4.

Expressions for these diagrams can be written immediately using the rules of the old-fashioned perturbation theory. According to these rules each time-ordered diagram corresponds to an integral over the internal three-momenta, the integrand being a product of the terms of the type

$$\left[P_0 - \sum_i E_i - \sum_j \omega_j + i\epsilon \right]^{-1} ,$$

each term corresponding to a vertical crossing line as in Fig. 4. Here P_0 is the total energy of the two-body system, and E_i and ω_j are the energies of the crossed nucleon and meson lines, respectively; the energies of the internal particles being taken on shell. However, in our case, energies of the external particles can be on or off the mass shell. There is an additional factor of the type $(2E_{\vec{Q}''}P_0)^{-1}$ for each pair of internal nucleons arising due to our approximation (2.10).[12] The separation of V into V_+ and V_- gives rise to extra factors of the type $g^2(2\omega_{\vec{Q}-\vec{Q}'})^{-1}$ for each meson line [see Eq. (2.11)]. Finally a factor of $(2\pi)^{-3}$ is to be included with each independent internal three-momentum being integrated over.

The Q_0'' integration in the remaining three terms in Eq. (2.12) can be performed similarly, leading to additional time-ordered diagrams as in Fig. 5. Thus the "box" diagram in Fig. 2 gives rise to six time-ordered diagrams. In two out of the six diagrams there are two mesons present simultaneously in an intermediate state. These various possibilities arise essentially because the relativistic interaction is a retarding one.

The higher order terms in the Born series in Fig. 2 can be treated identically. For example, the third term $VGVGV$ can be rewritten as

$$(V_+ + V_-)G(V_+ + V_-)G(V_+ + V_-) .$$

The virtual energy integrations can be performed separately in each of the eight terms $V_\pm GV_\pm GV_\pm$. Again the final answer can be written as a sum of time-ordered diagrams of the old-fashioned perturbation theory. For instance, the term $V_+GV_+GV_+$ is equal to the sum of five diagrams, shown in Fig. 6.

Considering the complete set of time-ordered diagrams generated this way, we can separate them into iterative and noniterative blocks. We define an effective potential, $V^{\text{eff}}(P_0,Q,Q')$, as the sum of all noniterative diagrams. After regrouping the noniterative diagrams, V^{eff} can be rewritten as the sum of two terms[7]

$$V^{\text{eff}}(P_0,Q,Q') = V_+^{\text{eff}}(P_0,Q,Q') + V_-^{\text{eff}}(P_0,Q,Q') ,$$

where $V_\pm^{\text{eff}}$ are defined as in Fig. 7. Expressions for any of the diagrams in Fig. 7 can be written easily using the rules of the old-fashioned perturbation theory.

If the external nucleons crossed by vertical lines are taken on the mass shell, then the sum of all iterative and noniterative diagrams $\tilde{T}_{NN}(P_0,\vec{Q},\vec{Q}')$ can be written as the solution of the following Lippmann-Schwinger type of equation:

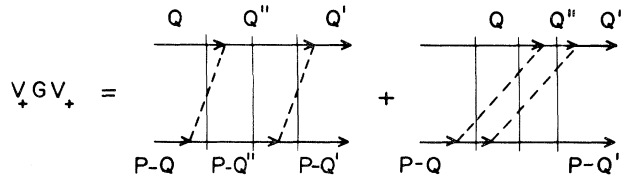

FIG. 4. Time-ordered diagrams resulting from V_+GV_+.

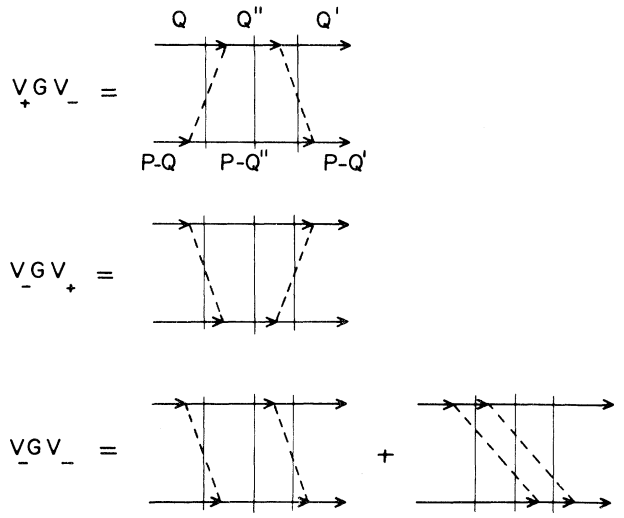

FIG. 5. Time-ordered diagrams resulting from V_+GV_-, V_-GV_+, and V_-GV_-.

$$\tilde{T}_{NN}(P_0,\vec{Q},\vec{Q}')=V^{\text{eff}}(P_0,\vec{Q},\vec{Q}')+\int \frac{V^{\text{eff}}(P_0,\vec{Q},\vec{Q}'')\tilde{T}_{NN}(P_0,\vec{Q}'',\vec{Q}')}{2P_0E_{\vec{Q}''}(P_0-2E_{\vec{Q}''}+i\epsilon)(2\pi)^3}d^3Q'' \ . \tag{2.15}$$

Thus, in the definition of V_+^{eff}, $Q_0=E_{\vec{Q}}$ and $Q_0'=P_0-E_{\vec{Q}'}$, and in the definition of V_-^{eff}, $Q_0=P_0-E_{\vec{Q}}$ and $Q_0'=E_{\vec{Q}'}$. Since we are working in the center of mass frame ($\vec{P}=0$), we have $V_+^{\text{eff}}=V_-^{\text{eff}}=(\frac{1}{2})V^{\text{eff}}$. The successive terms in the expansions for $V_\pm^{\text{eff}}=V_\pm^{(1)\text{eff}}+V_\pm^{(2)\text{eff}}+V_\pm^{(3)\text{eff}}+\cdots$ (Fig. 7) are

$$V_\pm^{(1)\text{eff}}(P_0,\vec{Q},\vec{Q}')=\frac{g^2}{2\omega_{\vec{Q}-\vec{Q}'}}\frac{1}{P_0-E_{\vec{Q}}-E_{\vec{Q}'}-\omega_{\vec{Q}-\vec{Q}'}+i\epsilon} \ , \tag{2.16}$$

$$V_\pm^{(2)\text{eff}}(P_0,\vec{Q},\vec{Q}')=g^4\int \frac{(8P_0E_{\vec{Q}''}\omega_{\vec{Q}-\vec{Q}''}\omega_{\vec{Q}''-\vec{Q}'})^{-1}(2\pi)^{-3}d^3Q''}{(P_0-E_{\vec{Q}}-E_{\vec{Q}''}-\omega_{\vec{Q}-\vec{Q}''}+i\epsilon)(P_0-E_{\vec{Q}}-E_{\vec{Q}'}-\omega_{\vec{Q}-\vec{Q}''}-\omega_{\vec{Q}''-\vec{Q}'}+i\epsilon)(P_0-E_{\vec{Q}''}-E_{\vec{Q}'}-\omega_{\vec{Q}'-\vec{Q}''}+i\epsilon)} \ , \tag{2.17}$$

$$\begin{aligned}V_\pm^{(3)\text{eff}}(P_0,\vec{Q},\vec{Q}')=g^6\int &\frac{(2P_0E_{\vec{Q}''})^{-1}(2P_0E_{\vec{Q}'''})^{-1}(8\omega_{\vec{Q}-\vec{Q}''}\omega_{\vec{Q}''-\vec{Q}'''}\omega_{\vec{Q}'''-\vec{Q}'})^{-1}(2\pi)^{-6}d^3Q''d^3Q'''}{(P_0-E_{\vec{Q}}-E_{\vec{Q}''}-\omega_{\vec{Q}-\vec{Q}''}+i\epsilon)(P_0-E_{\vec{Q}}-E_{\vec{Q}'''}-\omega_{\vec{Q}-\vec{Q}''}-\omega_{\vec{Q}''-\vec{Q}'''}+i\epsilon)}\\ &\times\left[\frac{1}{P_0-E_{\vec{Q}''}-E_{\vec{Q}'''}-\omega_{\vec{Q}''-\vec{Q}'''}+i\epsilon}\right.\\ &\left.+\frac{1}{P_0-E_{\vec{Q}}-E_{\vec{Q}'}-\omega_{\vec{Q}-\vec{Q}''}-\omega_{\vec{Q}''-\vec{Q}'''}-\omega_{\vec{Q}'''-\vec{Q}'}+i\epsilon}\right]\\ &\times\frac{1}{(P_0-E_{\vec{Q}''}-E_{\vec{Q}'}-\omega_{\vec{Q}''-\vec{Q}'''}-\omega_{\vec{Q}'''-\vec{Q}'}+i\epsilon)(P_0-E_{\vec{Q}'''}-E_{\vec{Q}'}-\omega_{\vec{Q}'''-\vec{Q}'}+i\epsilon)} \ .\end{aligned} \tag{2.18}$$

We thus obtain the auxiliary amplitude, $\tilde{T}_{NN}(P_0,\vec{Q},\vec{Q}')$, which is the sum of all iterative and noniterative diagrams with external nucleons crossed by vertical lines taken on shell. The Bethe-Salpeter amplitude

$$T_{NN}(P_0,Q_0,Q_0',\vec{Q},\vec{Q}')$$

on the other hand, is also the sum of all iterative and noniterative diagrams, but now the external nucleons can be off the mass shell. However, it is clear that

$$T_{NN}(P_0,Q_0,Q_0',\vec{Q},\vec{Q}')$$

can be connected with

$$\tilde{T}_{NN}(P_0,\vec{Q},\vec{Q}')$$

by the following relation (involving only three-dimensional integrals):

$$T_{NN}=V^{\text{eff}}+V^{\text{eff}}GV^{\text{eff}}+V^{\text{eff}}G\tilde{T}_{NN}GV^{\text{eff}} \ , \tag{2.19}$$

where the Green's function G is the same as in Eq. (2.15) and the effective potential

$$V^{\text{eff}}=V_+^{\text{eff}}+V_-^{\text{eff}} \ .$$

The potentials $V_\pm^{\text{eff}}$ are given by expansions in Fig. 7; however, unlike Eqs. (2.16)–(2.18), energies of the external nucleons can be off the mass shell.

Now using Eq. (2.19) we observe that the Bethe-Salpeter amplitude, T_{NN}, for *on-shell scattering*

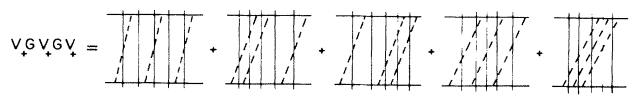

FIG. 6. Time-ordered diagrams resulting from $V_+GV_+GV_+$.

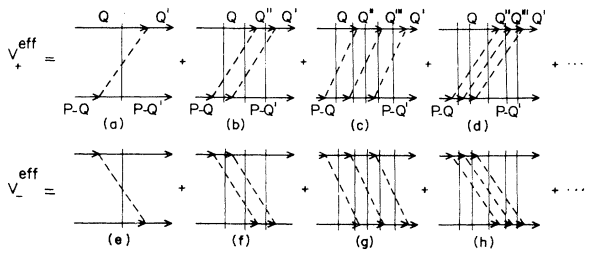

FIG. 7. Definition of the effective potential $V^{\text{eff}}=V_+^{\text{eff}}+V_-^{\text{eff}}$ in the ladder approximation.

($P_0=2E_{\vec{Q}}=2E_{\vec{Q}'}$, $Q_0=E_{\vec{Q}}$, $Q_0'=E_{\vec{Q}'}$) coincides with the amplitude $\tilde{T}_{NN}$ defined by Eq. (2.15).

$$T_{NN}^{\text{on shell}}=\tilde{T}_{NN}^{\text{on shell}} . \tag{2.20}$$

Therefore these amplitudes reproduce the same phase shift. This result is very important, since instead of solving the Bethe-Salpeter equation, to find the scattering amplitude, one can solve its three-dimensional analog. Of course the solution of Eq. (2.15) would be close to that of the Bethe-Salpeter equation only if the approximation in Eq. (2.10) is good. Also the practical utility of our method depends upon how fast the series for V^{eff} converges.

Equation (2.15) resembles the Gross equation, Eq. (2.8). However, the effective potential here is different from the potential in the Gross equation. Even the first term, Eq. (2.16), of the expansion for V^{eff} differs from the potential in the Gross equation, Eq. (2.8).

In the nonrelativistic limit the first term of the expansion for V^{eff}, Eq. (2.16), goes over to the nonrelativistic Yukawa potential, Eq. (1.2); the second term does not vanish but goes over to the two-meson exchange contribution in the NN potential, and so on. Thus unlike the Blankenbecler-Sugar and Gross equations, Eq. (2.15) has the desirable feature that in the nonrelativistic limit it allows for the multimeson exchange processes. We will return to the discussion of this limit later, after we generalize our formalism to include the crossed diagrams. We now present our numerical results and also compare the solution of the exact Bethe-Salpeter equation with those of the various three-dimensional approximations to it.

III. NUMERICAL RESULTS IN THE LADDER APPROXIMATION

Several authors have solved the Bethe-Salpeter equation for scalar "nucleons" exchanging scalar "bosons" and have calculated NN S-wave phase shifts as a function of two-nucleon energy.[10,11] We use here the recent results of Mueller and Gloeckle,[11] who solved the Bethe-Salpeter equation in the ladder approximation, and then also included the two-meson-exchange crossed-box diagram in the driving term. In this section, however, we restrict ourselves to the ladder approximation.

Mueller and Gloeckle in their calculations used many different values of the meson-nucleon constant and the exchanged meson mass. For the sake of comparison we use the same values in our calculations. The first set of calculations corresponds to the exchanged meson mass $\mu=m_\pi=138.13$ MeV, and the following four values of the coupling constant g:

$$\begin{aligned} g_a{}^2&=3.3563\times10^6\ \text{MeV}^2 ,\\ g_b{}^2&=1.0\times10^7\ \text{MeV}^2 ,\\ g_c{}^2&=3.0\times10^7\ \text{MeV}^2 ,\\ g_d{}^2&=7.0\times10^7\ \text{MeV}^2 . \end{aligned} \tag{3.1}$$

The parameter g_a has also been used by Woloshyn and Jackson[10] and it corresponds to a potential with strength of that of the one-pion-exchange part of the NN potential in the ${}^1S_0$ channel. The values g_c and g_d allow two-nucleon bound states.

The second set of calculations corresponds to the exchange of the fictitious σ meson: $\mu=500$ MeV. The values of the coupling constant are

$$\begin{aligned} g_b{}^2&=4.0\times10^7\ \text{MeV}^2 ,\\ g_c{}^2&=8.0\times10^7\ \text{MeV}^2 ,\\ g_d{}^2&=16.0\times10^7\ \text{MeV}^2 . \end{aligned} \tag{3.2}$$

Here a two-nucleon bound state is possible for g_c and g_d. For the nucleon we always use the physical mass $m=938.93$ MeV.

For numerical calculations we first performed the partial-wave projection of the integral equation (2.15). The Kowalski-Noyes method[13] was used to overcome the singularity in the kernel of the integral equation, thereby putting it in a Fredholm form. The Gauss-Legendre quadrature and matrix inversion methods were used to calculate the fully on-shell t matrix and thus the NN scattering phase shifts.

Results of our calculations are presented in Figs. 8—14, where we also compare our results with those based on the Bethe-Salpeter, Blankenbecler-Sugar, and Gross equations. The crosses represent the Bethe-Salpeter phase shifts obtained in the ladder approximation, Eqs. (1.4) and (1.5), and are taken from Ref. 11. The Blankenbecler-Sugar (Gross) results, Eq. (2.7) [Eq. (2.8)], are denoted by BBS1 (G1).

We begin our calculations of S-wave phase shifts with $V^{\text{eff}}=V^{(1)\text{eff}}$ [Eq. (2.16)], which is the first term of the expansion for the effective potential [Fig. 7(a)]. Recall that in the c.m. frame $V_+^{\text{eff}}=V_-^{\text{eff}}$. The corresponding results are denoted by $P1$ in Figs. 8—14. It is clear that when the coupling constant corresponds to the one-pion exchange potential in the ${}^1S_0$ nucleon-nucleon channel (Fig. 8), our result ($P1$) is in much better agreement with the Bethe-Salpeter phase shifts than are the Blankenbecler-Sugar and Gross results (BBS1, G1). The same is true also for a stronger coupling constant; see Fig. 9. If the coupling constant is increased further, so that a two-nucleon bound state is possible (Figs. 10 and 11), the agreement of our result ($P1$) with the

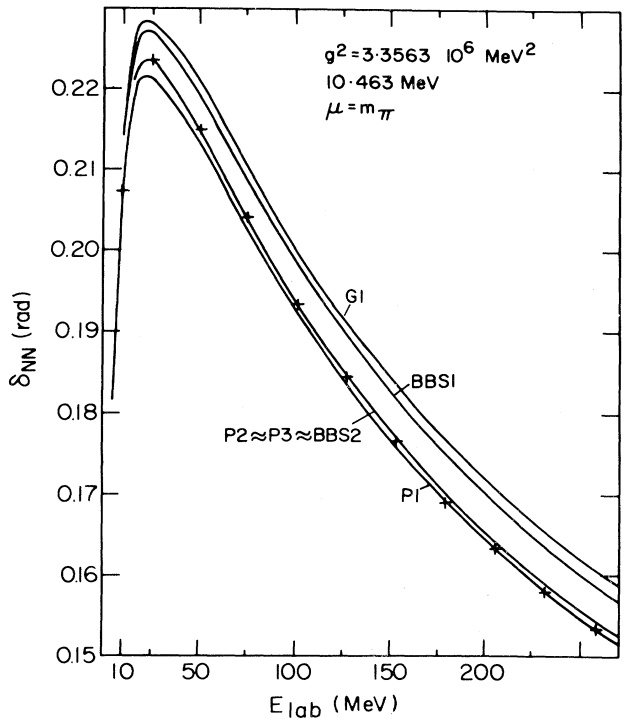

FIG. 8. Calculated NN phase shifts in radians versus laboratory kinetic energy in MeV. Crosses represent Bethe-Salpeter results in the ladder approximation and are taken from Ref. 11. Curves are described in the text. The meson-N coupling constant, the equivalent strength of the potential, and the mass of the exchanged meson are given in the upper right-hand corner.

Bethe-Salpeter phase shifts is about as good as that of the Blankenbecler-Sugar results (BBS1), but is much better than that of the Gross results (G1). The same general features are observed also in Figs. 12—14, where we consider a larger exchanged-meson mass ($\mu = 500$ MeV). For a relatively weak coupling constant (Fig. 12), our result ($P1$) is better than BBS1 and G1. For stronger coupling constants which allow two-nucleon bound states (Figs. 13 and 14), $P1$ is about as good as BBS1 but is better than G1.

Next we include the second term (of order g^4) in the effective potential so that

$$V^{\text{eff}} = V^{(1)\text{eff}} + V^{(2)\text{eff}} ,$$

[see Fig. 7(b) and Eq. (2.17)]. This term corresponds to a two-meson exchange contribution in the effective potential. A large part of the calculation of $V^{(2)\text{eff}}$ for the S wave can be done analytically as described in Appendix A. The results of our calculations, which include $V^{(2)\text{eff}}$, are denoted by $P2$ in Figs. 8—14. First, if we have $\mu = m_\pi$ for relatively weak coupling constants (Figs. 8 and 9), the inclusion of $V^{(2)\text{eff}}$ does not affect the phase shifts very much. For stronger coupling constants, however, it makes a significant contribution, thereby improving the agreement of our results ($P2$) with the Bethe-Salpeter phase shifts (Figs. 10 and 11). Similar remarks can be made about Figs. 12—14, where

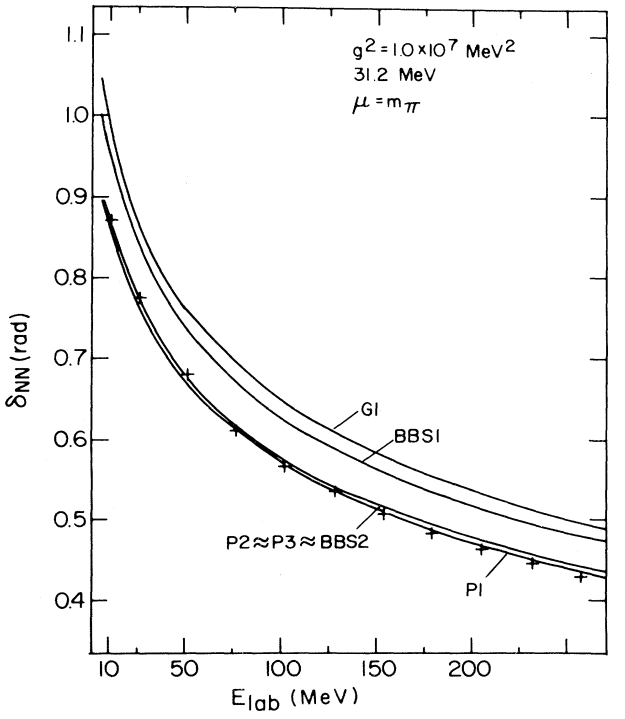

FIG. 9. See the caption to Fig. 8.

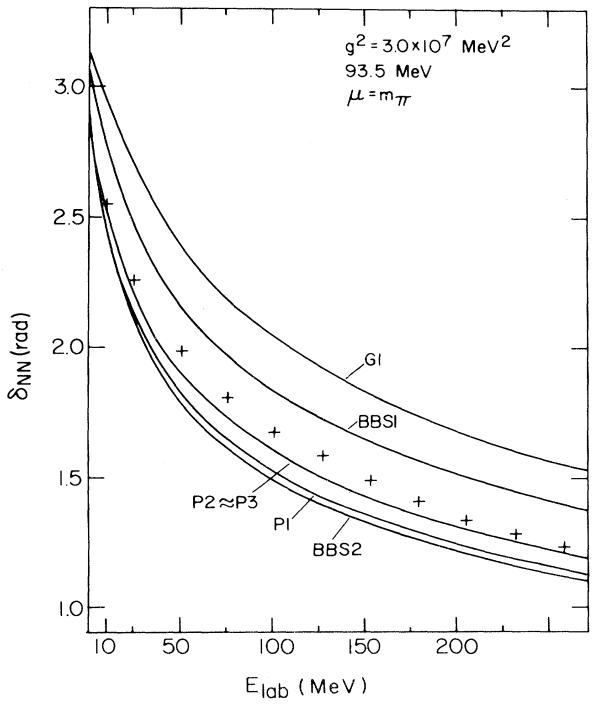

FIG. 10. See the caption to Fig. 8.

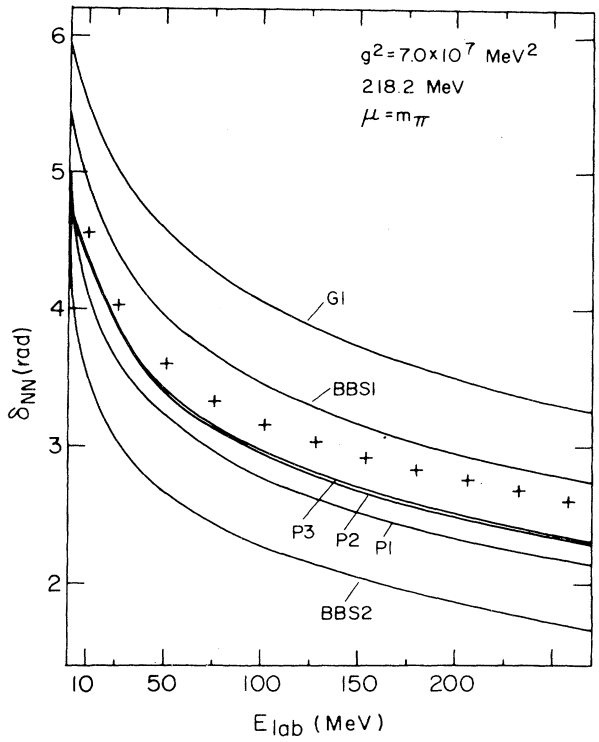

FIG. 11. See the caption to Fig. 8.

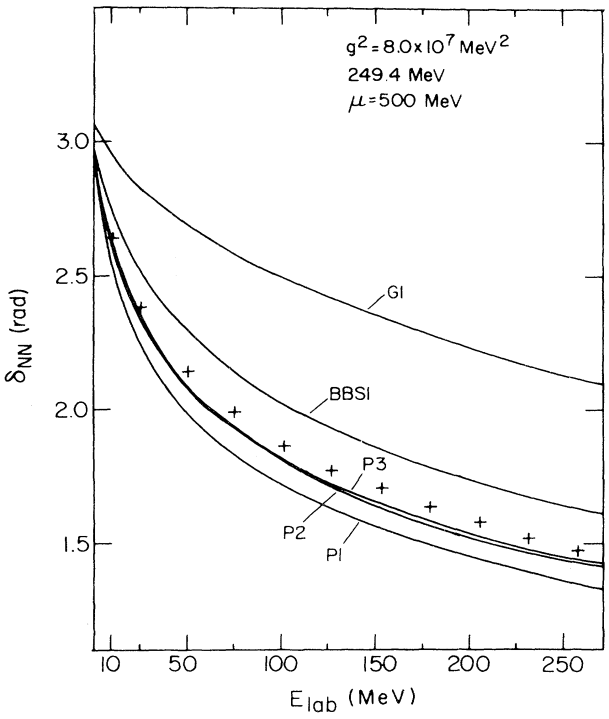

FIG. 13. See the caption to Fig. 8.

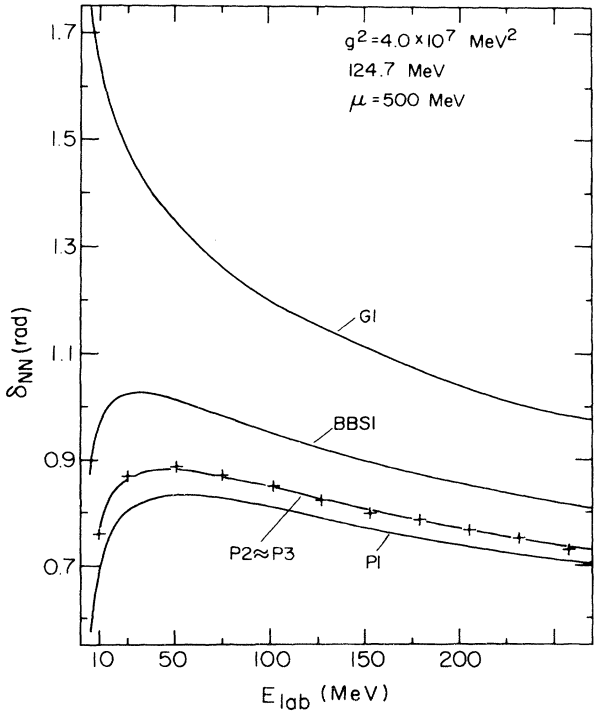

FIG. 12. See the caption to Fig. 8.

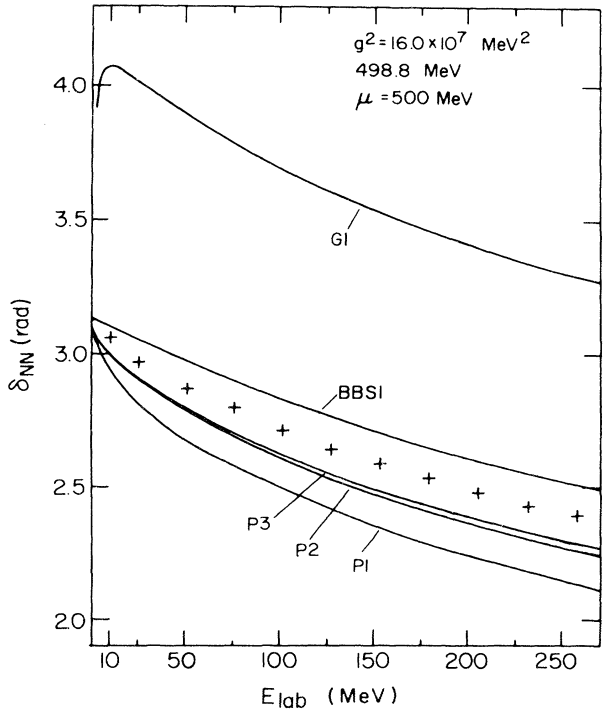

FIG. 14. See the caption to Fig. 8.

we have $\mu=500$ MeV. In Fig. 12, the inclusion of $V^{(2)\text{eff}}$ in the effective potential brings our results ($P2$) to a very good agreement with the Bethe-Salpeter phase shifts. For stronger coupling constants also, $V^{(2)\text{eff}}$ makes an important contribution, bringing our results closer to the Bethe-Salpeter phase shifts (Figs. 13 and 14).

The next term in V^{eff} (of order g^6), Eq. (2.18), corresponds to the three-meson exchange contribution in the effective potential [Figs. 7(c) and (d)]. The calculation of this term, after partial wave projection, involves a seven-dimensional integral. However, to a large extent it can be done analytically, as described in Appendix B. Finally, there remains a three-dimensional integral, which we evaluate numerically. The results of our calculations with

$$V^{\text{eff}}=V^{(1)\text{eff}}+V^{(2)\text{eff}}+V^{(3)\text{eff}}$$

are denoted as $P3$ in Figs. 8—14. We see that the influence of $V^{(3)\text{eff}}$ is very small in all figures, indicating a very rapid convergence of our series for V^{eff} even for rather large coupling constants. The convergence of the series for V^{eff}, in the nonrelativistic limit, was roughly estimated in Ref. 7. We found there that the parameter of expansion is of the order $g^2/(2\pi)^3m^2$.

Despite an overall agreement of our results ($P3$) with the Bethe-Salpeter S-wave phase shifts, it is clear from Figs. 8—14 that for a fixed μ as the strength of the potential increases the agreement becomes worse. A possible explanation for the disagreement is the neglect of the negative energy nucleon poles in our treatment.

Now considering the potentials in the Blankenbecler-Sugar and Gross equations [Eqs. (2.7) and (2.8)] as the first terms of an infinite series, Eq. (2.4), one can calculate the first correction term $V(G-g)V$. Results of such a calculation with a modified potential $W=V+V(G-g)V$ are given in Ref. 11 only for the case of the Blankenbecler-Sugar equation and the potentials in Eq. (3.1). These results are denoted by BBS2. We see in Figs. 8 and 9 that the inclusion of this term (which involves a four-dimensional integral) improves the phase shift calculated with the Blankenbecler-Sugar equation and it almost coincides with our result, $P1$, obtained with $V^{\text{eff}}=V^{(1)\text{eff}}$, Eq. (2.16). However, for larger coupling constants (Figs. 10 and 11), the inclusion of the term $V(G-g)V$ does not improve the results at all. In fact it leads to worsening of the results, as we see in Fig. 11. This probably indicates poor convergence of the expansion (2.4) at least up to the order studied, if one uses the Blankenbecler-Sugar choice of g. Also note that in Figs. 10 and 11 the curves $P2$ are in much better agreement with the crosses than are the curves BBS2.

A very large body of literature exists in which a theoretical reduction scheme and a phenomenological boson-exchange potential are chosen to fit the empirical NN phase shift data and thus generate a set of phenomenological meson masses and meson-nucleon coupling constants. These in turn are used in extensive nuclear matter and nuclear structure calculations. It is important to study how sensitive these coupling constants and meson masses are to the choice of the reduction scheme.[14] So we performed a simple calculation in which the Bethe-Salpeter results in Figs. 12—14 were treated as experimental data and the theoretical approaches labeled BBS1, G1, and $P1$ were used in turn to fit these "data" by adjusting the meson-N coupling constant and the meson mass. Minimum-χ^2 fits were obtained, thereby determining the "mass" of the fictitious σ meson and the σN "coupling constant." Results are presented in Tables I—III. Numbers in the first column are the values of χ^2 corresponding to the various curves shown in Figs. 12—14. The second column gives the minimum χ^2 corresponding to the best-fit curves. The next two columns give the fitted g^2 and μ. Since the various

TABLE I. σN coupling constant and σ meson mass obtained by performing minimum-χ^2 fits to the Bethe-Salpeter results in Fig. 12. $g^2=4.0\times10^7$ MeV^2 and $\mu=500$ MeV.

	χ_{init}^2	$\chi_{\text{fi}}^2\equiv\chi_{\text{min}}^2$	Fitted g^2 MeV^2	Fitted μ MeV
BBS1	0.155	1.22×10^{-4}	3.54×10^7	479
G1	2.097	1.74×10^{-4}	3.06×10^7	464
$P1$	0.019	1.28×10^{-4}	4.22×10^7	508

TABLE II. Same as Table I but for Fig. 13. $g^2=8.0\times10^7$ MeV^2 and $\mu=500$ MeV.

	χ_{init}^2	$\chi_{\text{fi}}^2\equiv\chi_{\text{min}}^2$	Fitted g^2 MeV^2	Fitted μ MeV
BBS1	0.237	4.92×10^{-4}	6.62×10^7	451
G1	3.807	5.06×10^{-4}	6.07×10^7	587
$P1$	0.221	5.57×10^{-4}	8.39×10^7	449

TABLE III. Same as Table I but for Fig. 14. $g^2=16.0\times10^7$ MeV^2 and $\mu=500$ MeV.

	χ_{init}^2	$\chi_{\text{fi}}^2\equiv\chi_{\text{min}}^2$	Fitted g^2 MeV^2	Fitted μ MeV
BBS1	0.133	3.37×10^{-4}	14.3×10^7	487
G1				
$P1$	0.522	3.76×10^{-4}	19.7×10^7	508

reduction schemes tested here treat the nucleon and meson as scalar particles, and since the crosses in Figs. 12—14 are not the true experimental data, the fitted g^2 and μ obviously have no physical significance. However, they serve an important purpose to demonstrate the sensitivity of the fitted parameters to the theoretical reduction scheme chosen. If this sensitivity persists in realistic calculations trying to fit the actual experimental data, then the phenomenological coupling constants and meson masses emerging from these calculations are of limited applicability.

IV. CROSSED DIAGRAMS AND NONRELATIVISTIC LIMIT OF THE BETHE-SALPETER EQUATION

Consider now the more general case where the driving term in the Bethe-Salpeter equation, V_{NN}, includes the "crossed-box" diagram (Fig. 15). As before we replace V by $V_+ + V_-$ in the expression for the crossed-box diagram, make the approximation (2.10), and then perform the Q_0'' integration separately in each of the four terms $V_\pm G V_\pm$. As in Sec. II this leads, after some algebra, to six terms which can be represented schematically as time-ordered diagrams (Fig. 16). Expressions for these diagrams can also be written using the rules of the old-fashioned perturbation theory described in Sec. II. Consider, for example, the diagram in Fig. 16(a). As in the case of Fig. 7, we take the external nucleons crossed by vertical lines on the mass shell (i.e., in the center-of-mass frame $Q_0 = P_0 - E_{\vec{Q}}$ and $Q_0' = P_0 - E_{\vec{Q}'}$). The expression for this diagram is

$$V_a^{\rm cr}(P_0,\vec{Q},\vec{Q}') = g^4 \int \frac{(8P_0 E_{\vec{Q}''}\omega_{\vec{Q}-\vec{Q}''}\omega_{\vec{Q}''-\vec{Q}'})^{-1}(2\pi)^{-3}d^3Q''}{(P_0 - E_{\vec{Q}} - E_{\vec{Q}''} - \omega_{\vec{Q}-\vec{Q}''} + i\epsilon)(P_0 - E_{\vec{Q}''} - E_{\vec{Q}+\vec{Q}'-\vec{Q}''} - \omega_{\vec{Q}-\vec{Q}''} - \omega_{\vec{Q}''-\vec{Q}'} + i\epsilon)(P_0 - E_{\vec{Q}''} - E_{\vec{Q}'} - \omega_{\vec{Q}''-\vec{Q}'} + i\epsilon)} . \tag{4.1}$$

Similarly, expressions for diagrams in Figs. 16(b) and (c) are

$$V_b^{\rm cr}(P_0,\vec{Q},\vec{Q}') = g^4 \int \frac{(8P_0 E_{\vec{Q}}\omega_{\vec{Q}-\vec{Q}''}\omega_{\vec{Q}''-\vec{Q}'})^{-1}(2\pi)^{-3}d^3Q''}{(P_0 - E_{\vec{Q}} - E_{\vec{Q}+\vec{Q}'-\vec{Q}''} - \omega_{\vec{Q}''-\vec{Q}'} + i\epsilon)(P_0 - E_{\vec{Q}''} - E_{\vec{Q}+\vec{Q}'-\vec{Q}''} - \omega_{\vec{Q}-\vec{Q}''} - \omega_{\vec{Q}''-\vec{Q}'} + i\epsilon)(P_0 - E_{\vec{Q}''} - E_{\vec{Q}'} - \omega_{\vec{Q}''-\vec{Q}'} + i\epsilon)} , \tag{4.2}$$

$$V_c^{\rm cr}(P_0,\vec{Q},\vec{Q}') = g^4 \int \frac{(8P_0 E_{\vec{Q}''}\omega_{\vec{Q}-\vec{Q}''}\omega_{\vec{Q}''-\vec{Q}'})^{-1}(2\pi)^{-3}d^3Q''}{(P_0 - E_{\vec{Q}} - E_{\vec{Q}+\vec{Q}'-\vec{Q}''} - \omega_{\vec{Q}''-\vec{Q}'} + i\epsilon)(P_0 - E_{\vec{Q}} - E_{\vec{Q}'} - \omega_{\vec{Q}-\vec{Q}''} - \omega_{\vec{Q}''-\vec{Q}'} + i\epsilon)(P_0 - E_{\vec{Q}''} - E_{\vec{Q}'} - \omega_{\vec{Q}''-\vec{Q}'} + i\epsilon)} . \tag{4.3}$$

It is easy to see that, in the center-of-mass frame, the diagrams in Figs. 16(d)—(f) are equal to those in Fig. 16(a)—(c), respectively.

Now we are in a position to extend the definition of the effective potential given in Fig. 7. A more general definition that includes time-ordered diagrams resulting because of the inclusion of the crossed-box diagram in V_{NN} is given in Fig. 17. We recall that the effective potential should include all noniterative diagrams.

The solution of the Bethe-Salpeter equation, T_{NN}, can again be written in terms of an auxiliary amplitude $\tilde{T}_{NN}$ as in Sec. II, with $V^{\rm eff}$ in Eqs. (2.15) and (2.19) replaced by $V^{\rm eff}$ defined in Fig. 17. Recall that $V^{\rm eff}$ appearing in Eq. (2.15) has the external nucleons crossed by vertical lines on the mass shell (Fig. 7), while $V^{\rm eff}$ in Eq. (2.19) has no such restriction. A similar statement holds true in the case of Fig. 17 also. As before T_{NN} coincides with $\tilde{T}_{NN}$ in the on-shell case.

The results of our calculations of S-wave NN phase shifts when crossed diagrams are included in the effective potential are shown in Figs. 18—24. The same coupling constants and meson masses as in Sec. III were used [see Eqs. (3.1) and (3.2)]. The curves $P4$ correspond to the solution of Eq. (2.15), when the effective potential includes diagrams in Figs. 17(a)—(g). The curves $P5$ include, in addition, four diagrams of the type of Fig. 17(h) and four diagrams of the type of Fig. 17(i). The calculation of $P5$ will be explained in detail later. Crosses in Figs. 18—24 represent Bethe-Salpeter results obtained with V_{NN} in Fig. 15 and are taken from Ref. 11. The curves BBS3 are Blankenbecler-Sugar results, also taken from Ref. 11, and are based on the potential

$$W = V^{(2)} + V^{(2)}(G - g)V^{(2)} + V^{(4)}$$

[see Eq. (2.3)]. Here $V^{(2)}$ refers to Fig. 15(a) and $V^{(4)}$ to Fig. 15(b), where both nucleons are either on

shell or equally off shell. Curves labeled G1 and BBS1 are Gross and Blankenbecler-Sugar results in the ladder approximation, and are the same as in Figs. 8—14.

We see from Figs. 18—20 that the agreement of our results with the Bethe-Salpeter results is good, even for a rather strong coupling constant in Fig. 20. However, in Fig. 21, where we have a stronger coupling constant for the same exchanged meson mass, the agreement is not so good. This is somewhat surprising since for comparable or even stronger coupling constants in Figs. 22—24, the disagreement of curves $P5$ with the crosses is much smaller. (Note that scales are different in various figures.) Besides the neglect of the negative energy nucleon poles in the present calculations, this disagreement could also be due to numerical uncertainties in the solution of the Bethe-Salpeter equation.[11]

The curves BBS3 in Figs. 18—21 are very close to the curves BBS1 in Figs. 8—11, respectively. This is due to cancellation between $V^{(4)}$ and $V^{(2)}(G-g)V^{(2)}$ terms in the potential W in the limit $\mu/m\to 0$.[11] This cancellation, which occurs in some models,[11] improves the convergence of the series (2.4) if the potential V_{NN} includes the crossed diagram (Fig. 15). This may explain why the agreement between the Blankenbecler-Sugar and Bethe-Salpeter results is good for small coupling constants. The same cancellation (in the limit $\mu/m\to 0$) also occurs in the Gross equation[5,9] and may explain the good agreement between G1 and the Bethe-Salpeter phase shifts in Figs. 18 and 19. [Unfortunately, Mueller and Gloeckle[11] present their results obtained with

$$W=V^{(2)}+V^{(2)}(G-g)V^{(2)}+V^{(4)}$$

only in the case of the Blankebecler-Sugar equation and for coupling constants in Eq. (3.1) only.]

Consider now the nonrelativistic limit of our equations in the ladder approximation. We have shown earlier that in this limit the Blankenbecler-Sugar and Gross equations go over to the Lippmann-Schwinger equation with the nonrelativistic Yukawa potential as the driving term. Our equation (2.15) also goes over to the Lippmann-Schwinger equation, but with a potential that is different from the nonrelativistic Yukawa potential. Only the first term in the expansion for $V^{\rm eff}$ (Fig. 7) goes over to the nonrelativistic Yukawa potential. Thus if

$$P_0-E_{\vec{Q}}-E_{\vec{Q}'}\ll\omega_{\vec{Q}-\vec{Q}'}$$

we obtain from Eq. (2.16) that

$$V^{(1)\rm eff}=V_+^{(1)\rm eff}+V_-^{(1)\rm eff}\to\frac{-g^2}{\omega_{\vec{Q}-\vec{Q}'}^{\,2}}$$

$$\equiv\frac{-g^2}{(\vec{Q}-\vec{Q}')^2+\mu^2}\ .$$

However, the second and higher order terms in the expansion for $V^{\rm eff}$ do not vanish in this limit. For example, for $V^{(2)\rm eff}$, Eq. (2.17), we find

$$V^{(2)\rm eff}\to-2g^4\int\frac{(4m)^{-2}(2\pi)^{-3}d^3Q''}{\omega_{\vec{Q}-\vec{Q}''}^{\,2}\omega_{\vec{Q}''-\vec{Q}'}^{\,2}(\omega_{\vec{Q}-\vec{Q}''}+\omega_{\vec{Q}''-\vec{Q}'})}\ . \tag{4.4}$$

For the three-meson exchange contribution, $V^{(3)\rm eff}$, Eq. (2.18), we find in this limit

$$V^{(3)\rm eff}\to-2g^6\int\frac{2(4m)^{-4}(2\pi)^{-6}d^3Q''d^3Q'''}{\omega_{\vec{Q}-\vec{Q}''}^{\,2}(\omega_{\vec{Q}-\vec{Q}''}+\omega_{\vec{Q}''-\vec{Q}'''})\omega_{\vec{Q}''-\vec{Q}'''}(\omega_{\vec{Q}''-\vec{Q}'''}+\omega_{\vec{Q}'''-\vec{Q}'})\omega_{\vec{Q}'''-\vec{Q}'}^{\,2}}$$
$$\times\left[\frac{1}{\omega_{\vec{Q}''-\vec{Q}'''}}+\frac{1}{\omega_{\vec{Q}-\vec{Q}''}+\omega_{\vec{Q}''-\vec{Q}'''}+\omega_{\vec{Q}'''-\vec{Q}'}}\right]\ . \tag{4.5}$$

Since the nonrelativistic interaction is instantaneous, the two- and three-meson exchange processes in Fig. 7 simply go over to instantaneous exchanges of two or three mesons at the same time. Schematically this may be represented as in Fig. 25.

Consider now the crossed diagrams in Fig. 17 in the same limit. We find from Eqs. (4.1)—(4.3) that

$$V_a^{\rm cr}\to-g^4\int\frac{(4m)^{-2}(2\pi)^{-3}d^3Q''}{\omega_{\vec{Q}-\vec{Q}''}^{\,2}\omega_{\vec{Q}''-\vec{Q}'}^{\,2}(\omega_{\vec{Q}-\vec{Q}''}+\omega_{\vec{Q}''-\vec{Q}'})} \tag{4.6}$$

and

$$V_b^{\rm cr}\text{ and }V_c^{\rm cr}\to-g^4\int\frac{(4m)^{-2}(2\pi)^{-3}d^3Q''}{\omega_{\vec{Q}-\vec{Q}''}\omega_{\vec{Q}''-\vec{Q}'}^{\,3}(\omega_{\vec{Q}-\vec{Q}''}+\omega_{\vec{Q}''-\vec{Q}'})}\ . \tag{4.7}$$

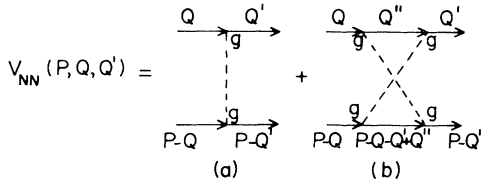

FIG. 15. Driving term in the Bethe-Salpeter equation including the crossed-box diagram.

Comparing Eqs. (4.6) and (4.7) with Eq. (4.4) we find that in this limit

$$V_+^{(2)\text{eff}} = V_a^{\text{cr}} \cong V_b^{\text{cr}} = V_c^{\text{cr}} . \tag{4.8}$$

In other words the second to fifth diagrams in Fig. 17 are all nearly equal. This makes sense, because if the interaction is instantaneous and if the potentials commute, then the order in which the mesons are absorbed or emitted is not important (see Fig. 26). Therefore in this limit the total contribution of the four diagrams of the order g^4 in Fig. 17 is simply four times the contribution of the stretched-box diagram [Eq. (4.4)], which obviates the need to calculate any of the three time-ordered crossed-box diagrams. We thus obtain that up to order g^4 the effective potential in Eq. (2.15), which includes all crossed diagrams, can be written as

$$V^{\text{eff}} \cong 2V_+^{(1)\text{eff}} + 8V_+^{(2)\text{eff}} , \tag{4.9}$$

where $V_+^{(1)\text{eff}}$ is given by Eq. (2.16) and $V_+^{(2)\text{eff}}$ by Eq. (2.17).

We do not make the approximation (4.9) in our calculations. However, to check it numerically, we solved Eq. (2.15) first with

$$V^{\text{eff}} = 2(V_+^{(1)\text{eff}} + V_+^{(2)\text{eff}} + V_a^{\text{cr}} + V_b^{\text{cr}} + V_c^{\text{cr}}) \tag{4.10}$$

and then with the effective potential in Eq. (4.9) and compared the resulting S-wave phase shifts. Both results are in excellent agreement, even in the case of the strongest coupling constants (for $\mu = m_\pi$ and

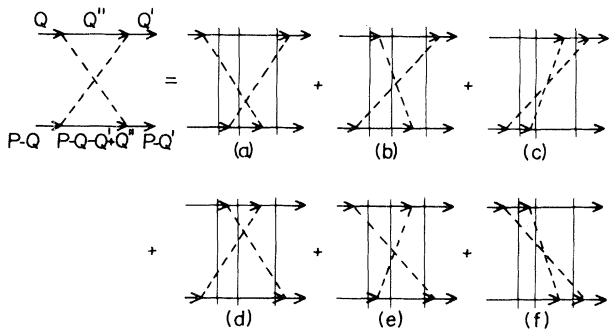

FIG. 16. Time-ordered diagrams resulting from the crossed-box diagram.

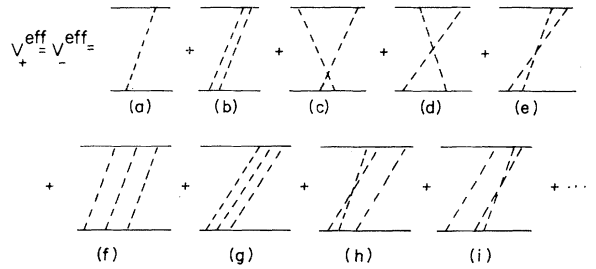

FIG. 17. Definition of the effective potential $V^{\text{eff}} = V_+^{\text{eff}} + V_-^{\text{eff}}$. In the c.m. frame $V_+^{\text{eff}} = V_-^{\text{eff}}$. (Compare with Fig. 7.)

$\mu = 500$ MeV) up to $E < 250$ MeV. (Only at $E \cong 250$ MeV there appear some deviations between these results in the case where $\mu = 500$ MeV.) The reason that this approximation is so good for rather large energies [although it was obtained in the strictly nonrelativistic limit, Eqs. (4.6)—(4.8) and Fig. 26] is the following. We can see that the restrictions (2.9) and

$$P_0 - E_{\vec{Q}} - E_{\vec{Q}'} \ll \omega_{\vec{Q}-\vec{Q}'}$$

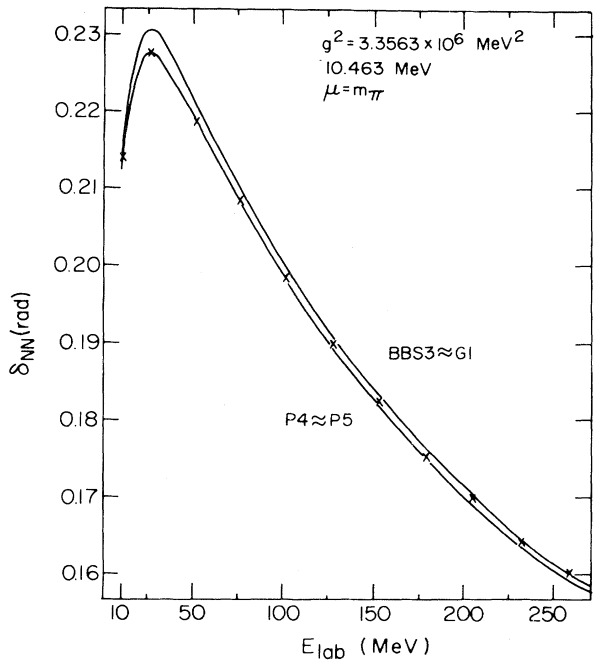

FIG. 18. Calculated NN phase shifts in radians versus laboratory kinetic energy in MeV. Crosses represent Bethe-Salpeter results with the driving term V_{NN} as in Fig. 15 and are taken from Ref. 11. Curves are described in the text. The meson-N coupling constant, the equivalent strength of the potential, and the mass of the exchanged meson are given in the upper right-hand corner.

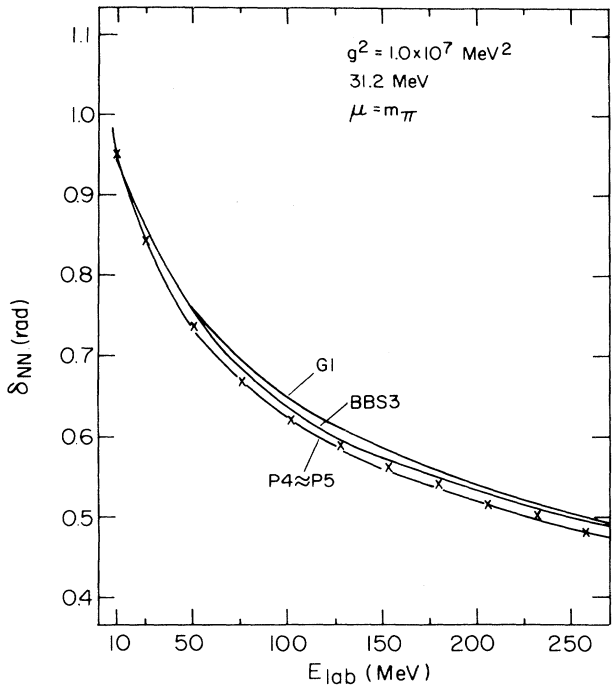

FIG. 19. See the caption to Fig. 18.

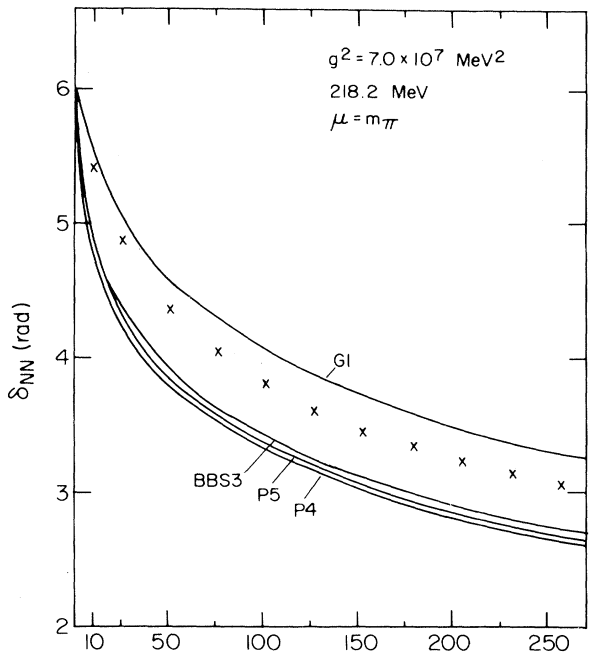

FIG. 21. See the caption to Fig. 18.

could be lifted and the approximation (4.8) can still remain valid. Indeed in the integrals (2.17) and (4.1)—(4.3) one can approximate the energies of virtual nucleons by $P_0/2$, i.e.,

$$E_{\vec{Q}''} \cong E_{\vec{Q}+\vec{Q}'-\vec{Q}''} \cong P_0/2 ,$$

which means that the energy is equally distributed between the two virtual nucleons (similar to the procedure of Blankenbecler and Sugar). In this case also one can see that the relation (4.8) holds.

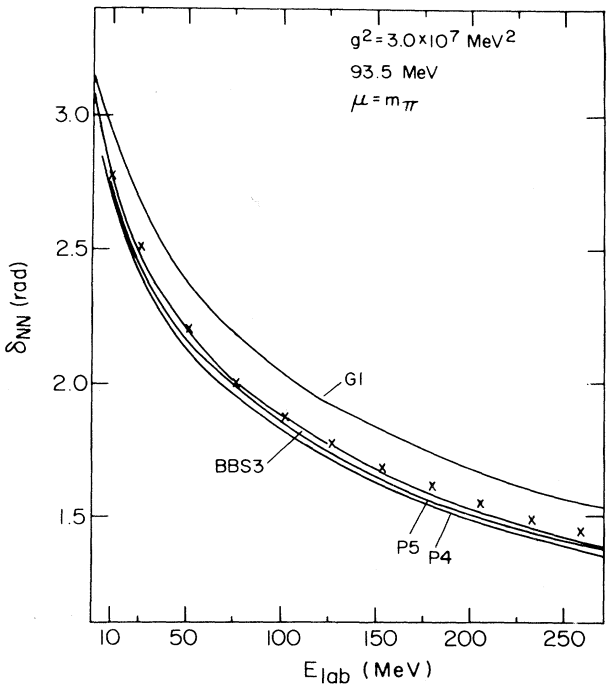

FIG. 20. See the caption to Fig. 18.

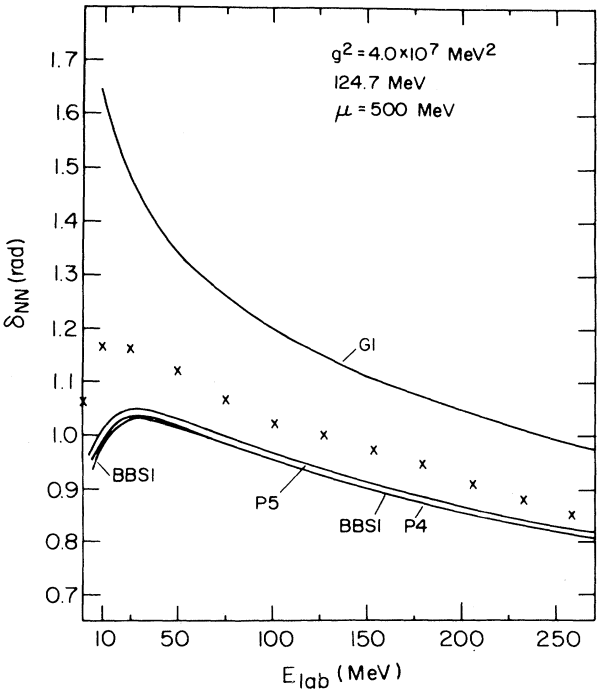

FIG. 22. See the caption to Fig. 18.

The approximate relation between the box and the crossed-box diagrams [Eq. (4.8), Fig. 26] is an important result valid in the low energy region. It provides us with a new method for a simpler evaluation of any crossed diagrams in V^{eff}, and therefore for a practical treatment of the Bethe-Salpeter equation with complicated crossed diagrams in the driving term.

Consider, for example, the three-meson exchange contribution in V^{eff}. Note that in this case we cannot compare our results with Bethe-Salpeter phase shifts since we do not know any calculations with the Bethe-Salpeter equation, where the driving term is calculated up to order g^6. Nevertheless, in the calculations of Mueller and Gloeckle,[11] the driving term (Fig. 15) generates some terms of order g^6 in our potential V^{eff}. These terms correspond to diagrams (f)—(i) in Fig. 17, and another six diagrams of type (h) and (i) which are not shown in Fig. 17. We therefore take into account only these terms and compare our results with the Bethe-Salpeter phase shifts.

For evaluation of crossed diagrams of order g^6 we use the same idea as described above; that is, we first compare different diagrams in the nonrelativistic limit. We thus obtain that each crossed diagram of order g^6 can be approximated by a box diagram. However, in this case we have two box diagrams as shown in Figs. 7(c) and (d) [or (g) and (h)]. They correspond to two different kinds of processes; in

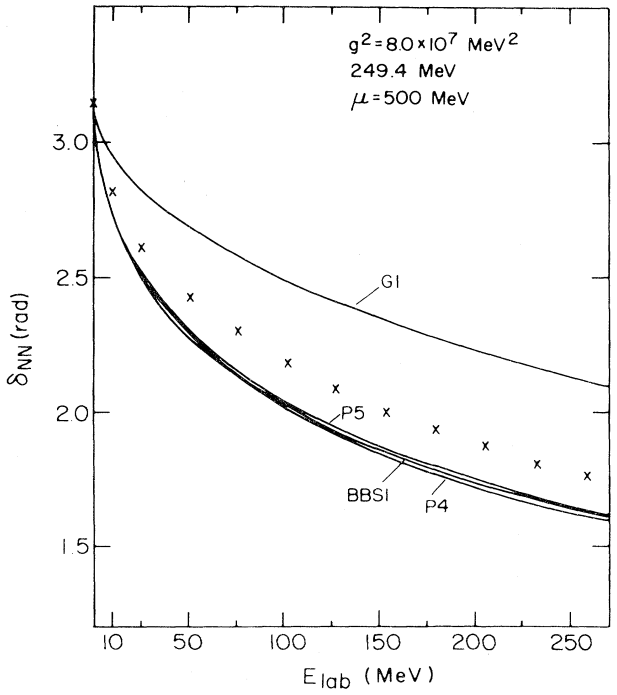

FIG. 23. See the caption to Fig. 18.

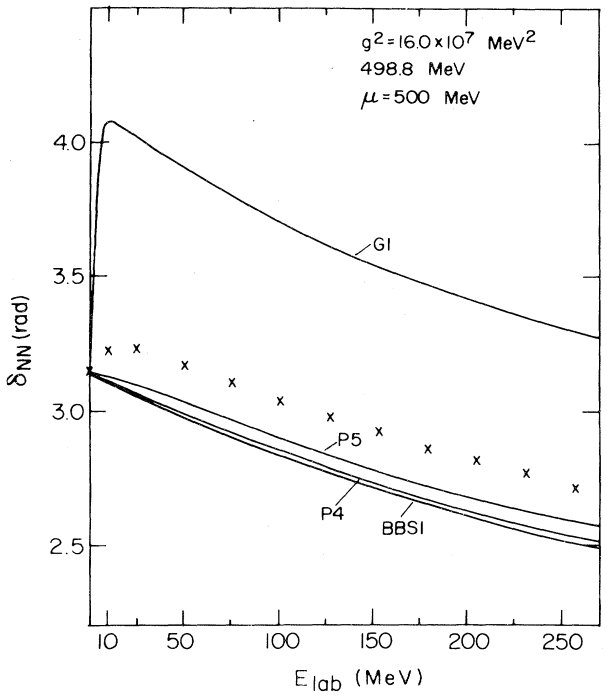

FIG. 24. See the caption to Fig. 18.

Fig. 7(c) we have no more than two mesons in any intermediate state, while in Fig. 7(d) we have a three meson intermediate state. The crossed diagrams are divided accordingly into two classes. In the case which we are considering there are eight crossed diagrams of the type in Figs. 17(h) and (i), out of which six are of the first class, and two of the second class. In the nonrelativistic limit, Eq. (4.5), we observe that a diagram of the second class (where three mesons are present simultaneously in an intermediate state) is approximately one-third of a diagram of the first class. We can thus approximate

$$V^{\text{eff}} = 2V_+^{(1)\text{eff}} + 8V_+^{(2)\text{eff}} + 16V_+'^{(3)\text{eff}} . \qquad (4.11)$$

Here $V_+'^{(3)\text{eff}}$ is given by Eq. (2.18), where only the first term in the square brackets is to be included. It corresponds to the contribution from the processes of the first class, where no more than two mesons appear in any intermediate state. The evaluation of this term is described in Appendix B.

Results of our calculation with V^{eff} given by Eq. (4.11) are presented in Figs. 18—24 as curves $P5$. We see that this part of the three meson-exchange contribution in the effective potential is important only when the coupling constants are large.

However, as mentioned above, the driving term, Fig. 15, of the Bethe-Salpeter equation does not generate all terms of order g^6 in our effective potential, V^{eff}. In fact, a much larger class of diagrams of order g^6 in V^{eff} exists; see for example, the diagrams

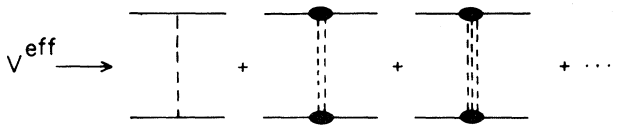

FIG. 25. Effective potential in Fig. 7 in the nonrelativistic limit. The blobs simply indicate that these diagrams are noniterative.

in Fig. 27. These diagrams are generated only if terms of order g^6 are included in the driving term of the Bethe-Salpeter equation. Their number can be found easily by counting all different configurations obtained by interchanging meson-NN vertices. We thus find that the number of all diagrams of order g^6 [including the two box diagrams, Figs. 17(f) and (g)] which contribute to $V_{\pm}^{\rm eff}$ is 40, where 16 of these diagrams belong to the first class and have no more than two mesons in any intermediate state. The remaining 24 diagrams contain three mesons in an intermediate state. Using our approximation, which relates these different diagrams, we find that $V^{\rm eff}$ which includes *all* processes of order g^6 is

$$V^{\rm eff}=2V_{+}^{(1)\rm eff}+8V_{+}^{(2)\rm eff}+48V_{+}^{\prime(3)\rm eff}\,, \qquad (4.12)$$

where $V_{+}^{\prime(3)\rm eff}$ is the same as in Eq. (4.11).

Results of our calculations with $V^{\rm eff}$ given by Eq. (4.12) are shown in Fig. 28 as curves $P6$. The upper three curves correspond to the strongest coupling constant in Eq. (3.1) with $\mu=m_\pi$ and the lower three to the strongest coupling constant in Eq. (3.2) with $\mu=500$ MeV. Curves $P1$ are the same as in Figs. 11 and 14, and curves $P'4$ are based on $V^{\rm eff}$ as in Eq. (4.10). We thus see that the three-meson exchange contribution may be quite important. The calculation of higher order terms in $V^{\rm eff}$ can be done in the same way. We, however, did not go beyond the three-meson exchange term in the present model calculations.

Here we described a simple method for evaluation of crossed diagrams in the effective potential. The derivation was presented for the particular case of scalar nucleons and scalar mesons. In this model the order in which mesons are absorbed or emitted is

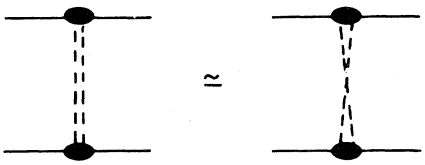

FIG. 26. Near equality of the box and crossed-box diagrams in the nonrelativistic limit.

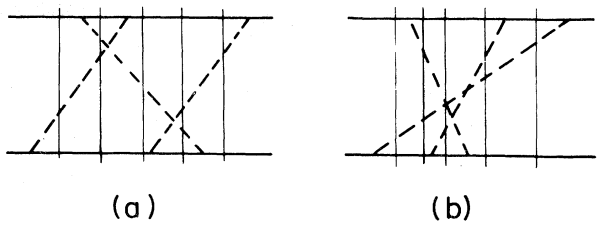

FIG. 27. An example of a three-meson exchange diagram (a) with no more than two mesons in any intermediate state, and (b) with a three-meson intermediate state.

not important (Fig. 26). However, in realistic calculations the interactions have parts which either commute or anticommute with each other. In the former case we will have relations of the type of Eq. (4.8). In the latter case we will have similar relations with opposite signs.

V. DISCUSSION

In this paper we derived a new three-dimensional approximation to the Bethe-Salpeter equation. The only approximation involved here is the neglect of the negative energy poles of the two-nucleon propa-

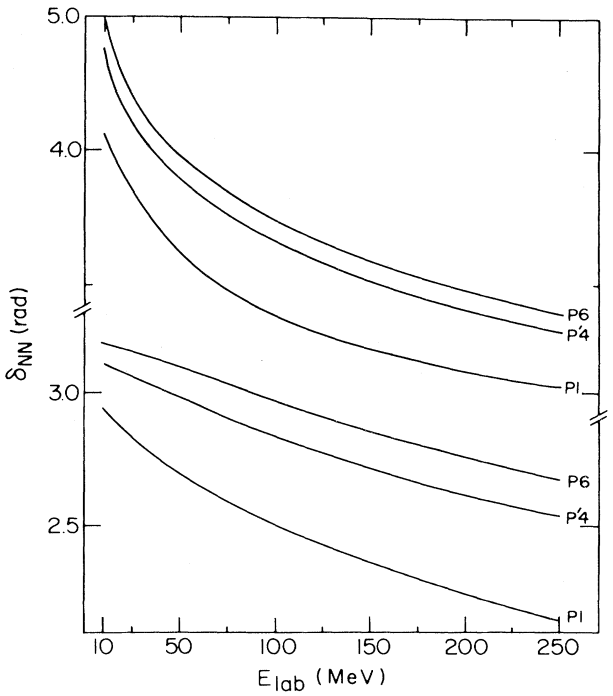

FIG. 28. Calculated NN phase shifts in radians versus laboratory kinetic energy in MeV. The curves are described in the text. The upper three curves correspond to $g^2=7.0\times10^7$ MeV^2 and $\mu=m_\pi$. The lower three curves correspond to $g^2=16.0\times10^7$ MeV^2 and $\mu=500$ MeV.

gator. Except for this point the phase shifts obtained with our equation and the Bethe-Salpeter equation would be identical. Although our equation has a simple form, similar to the Lippmann-Schwinger equation, it clearly displays the retarding nature of the relativistic interaction which is inherent in the Bethe-Salpeter equation. Using our results we investigated the nonrelativistic limit of the Bethe-Salpeter equation and found that the (relativistic) retardation effects do survive. Also in this limit the influence of the crossed diagrams in the driving term of the Bethe-Salpeter equation becomes transparent and it leads to an approximate method to take the contribution of these diagrams into account in a simple way. Using our results, which reveal important features of the Bethe-Salpeter equation, we now discuss their implication to works of other authors.

In a series of papers Tjon and collaborators[15] applied their new methods of numerical solution of the Bethe-Salpeter equation in the ladder approximation to the analysis of nucleon-nucleon phase shift data. They found that "the Bethe-Salpeter equation with one-boson exchange as the driving force is capable of giving a reasonable description of the nucleon-nucleon system."[16] However, as is clear from the present work, the use of the ladder approximation in the Bethe-Salpeter equation misses a major part of the multinucleon exchange contribution to the NN interaction. Therefore, the Bethe-Salpeter equation in the ladder approximation cannot be used for a systematic analysis of nucleon-nucleon data. Indeed, we demonstrated that the Bethe-Salpeter equation in the ladder approximation retains multimeson exchange forces even in the nonrelativistic limit, so that it differs from the usual Lippmann-Schwinger equation with the Yukawa potential. However, if this multimeson exchange contribution is important, one also needs to include cross diagrams in the driving term of the Bethe-Salpeter equation, since these diagrams generate the major part of the multimeson exchange contribution in any given order. For example, we have shown that in the two-meson exchange potential the contribution from the crossed diagrams is three times larger than the contribution from the stretched box diagram. If, however, the coupling constant is small, so that the multimeson forces are not important, then there is no advantage to using the Bethe-Salpeter equation instead of the Lippmann-Schwinger equation with the Yukawa potential.

A general question, what is the best relativistic equation for nuclear physics, has recently been discussed by Gross.[9] He arrived at a surprising conclusion that the Bethe-Salpeter equation is not the best equation. He argued that it does not satisfy a reasonable physical requirement, i.e., in the limiting case when the mass of one nucleon becomes very large, the Bethe-Salpeter equation does not go over to a one-body relativistic equation with an instantaneous potential (Gross refers to it as the "one-body limit"[9]). However, our analysis leads to an exactly opposite conclusion, namely the Bethe-Salpeter equation in the ladder approximation (this case was considered as the most pronounced example by Gross[9]) *has the one-body limit.* This can be easily seen from Eq. (2.15). The reason for the disagreement with Ref. 9 is as follows. Gross starts with the infinite ladder sum, which represents the solution of the Bethe-Salpeter equation in the ladder approximation. In order to find the three-dimensional potential he considers the energy integration in each of the ladder diagrams separately. However, his next step is only an observation that the second and higher order ladder diagrams after three-dimensional reduction contain some terms which are the iteration of the lower order term, and others which are not. The latter arise from the retarding terms in the potential (meson production singularities) and negative energy nucleon poles. Therefore he draws a conclusion that the infinite ladder sum cannot be written, even in the large mass limit, as an iteration of a three-dimensional potential, and thus the Bethe-Salpeter equation has one-body limit. In the present work we concentrated precisely on these "undesirable" terms. Although we considered only the meson production singularities and did not take into account negative energy nucleon poles, we found that the inclusion of these undesirable terms retains the one-body limit of the Bethe-Salpeter equation. Indeed, in the large mass limit these terms would correspond to the instantaneous multimeson exchange contribution in the effective three-dimensional potential. We therefore should include these undesirable terms in the definition of V^{eff}. Finally we obtain that the solution of the Bethe-Salpeter equation can indeed be represented as an iteration of V^{eff}, which is given by an infinite series, Fig. 7. Thus our conclusion is that the Bethe-Salpeter equation satisfies the Gross requirement, and it remains the best justified equation for nuclear physics.[2]

There is an interesting result about cancellation of the $V(G-g)V$ term, Eq. (2.4), in the large nucleon mass limit ($\mu/m \to 0$) when one uses the Gross or Blankenbecler-Sugar choice of g and includes the crossed-box diagram in the driving term of the Bethe-Salpeter equation.[5,9,11] These cancellations have been shown by Gross[9] to occur not only in the scalar case but also in the chiral theory of spin $\frac{1}{2}$ nucleons interacting with isovector pions. This has been considered as a justification for the one-boson-

exchange calculations of the NN potential.[11] However, in our opinion the underlying physics of these cancellations is not clear. Indeed, we obtain a similar, if not a better, agreement with the Bethe-Salpeter equation including crossed diagrams, Figs. 18–24, when no cancellation between multimeson exchange terms occurs.

APPENDIX A

The expression for the stretched-box diagram given in Eq. (2.17) after partial wave ($L=0$) projection has the form

$$\frac{g^4}{8\pi}\frac{(2\pi)^{-3}}{8P_0}\int \frac{(E_{\vec{Q}''}\omega_{\vec{Q}-\vec{Q}''}\omega_{\vec{Q}''-\vec{Q}'})^{-1}Q''^2dQ''d\cos\theta''d\phi''d\cos\theta'}{(\alpha-E_{\vec{Q}''}-\omega_{\vec{Q}-\vec{Q}''})(\beta-\omega_{\vec{Q}-\vec{Q}''}-\omega_{\vec{Q}''-\vec{Q}'})(\gamma-E_{\vec{Q}''}-\omega_{\vec{Q}'-\vec{Q}''})} ,$$

where $\alpha\equiv P_0-E_{\vec{Q}}$, $\beta\equiv P_0-E_{\vec{Q}}-E_{\vec{Q}'}$, $\gamma\equiv P_0-E_{\vec{Q}'}$, and θ' is the angle between $\vec{Q}$ and $\vec{Q}'$. In this appendix we briefly describe how two out of the four integrations in the above expression can be done analytically leaving only two for numerical work. The above integrand is nonsingular since we work below the pion production threshold. It is convenient to take the z axis along $\vec{Q}$ and introduce a redundant integration over ϕ' ($=0$ to 2π), the azimuthal angle of $\vec{Q}'$. It is clear that one may replace $d\Omega_{\vec{Q}'',\vec{Q}}d\Omega_{\vec{Q}',\vec{Q}}$ in the resulting expression by $d\Omega_{\vec{Q}'',\vec{Q}}d\Omega_{\vec{Q}',\vec{Q}''}$. Because of the special nature of the above integrand one may further replace $d\Omega_{\vec{Q}'',\vec{Q}}d\Omega_{\vec{Q}',\vec{Q}''}$ by $(2\pi)^2d\cos\theta''d\cos\psi$, where ψ is the angle between $\vec{Q}'$ and $\vec{Q}''$. Thus we get

$$\frac{g^4}{8\pi}\frac{(2\pi)^{-2}}{8P_0}\int \frac{(E_{\vec{Q}''}\omega_{\vec{Q}-\vec{Q}''}\omega_{\vec{Q}''-\vec{Q}'})^{-1}Q''^2dQ''dz_1dz_2}{(\alpha-E_{\vec{Q}''}-\omega_{\vec{Q}-\vec{Q}''})(\beta-\omega_{\vec{Q}-\vec{Q}''}-\omega_{\vec{Q}''-\vec{Q}'})(\gamma-E_{\vec{Q}''}-\omega_{\vec{Q}'-\vec{Q}''})} ,$$

where $z_1\equiv\cos\theta''$, $z_2\equiv\cos\psi$,

$$\omega_{\vec{Q}''-\vec{Q}}=(\mu^2+\vec{Q}''^2+\vec{Q}^2-2QQ''\cos\theta'')^{1/2} ,$$

$$\omega_{\vec{Q}''-\vec{Q}'}=(\mu^2+\vec{Q}''^2+\vec{Q}'^2-2Q'Q''\cos\psi)^{1/2} .$$

Integration over z_1 can be done analytically using standard techniques, leaving only two-dimensional integration to be done numerically.

APPENDIX B

In this appendix we briefly describe how the three-meson exchange diagram in Fig. 7(c) can be put in a numerically tractable form by performing many of the integrals analytically. After partial wave ($L=0$) projection, this diagram can be written as [see Eq. (2.18)]

$$\frac{g^6}{8\pi}\frac{(2\pi)^{-6}}{32P_0^2}\int \frac{(\omega_{\vec{Q}-\vec{Q}''}\omega_{\vec{Q}''-\vec{Q}'''}\omega_{\vec{Q}'''-\vec{Q}'}E_{\vec{Q}''}E_{\vec{Q}'''})^{-1}d^3Q''d^3Q'''d\cos\theta'}{(\alpha-E_{\vec{Q}''}-\omega_{\vec{Q}-\vec{Q}''})(\alpha-E_{\vec{Q}'''}-\omega_{\vec{Q}-\vec{Q}''}-\omega_{\vec{Q}''-\vec{Q}'''})(P_0-E_{\vec{Q}''}-E_{\vec{Q}'''}-\omega_{\vec{Q}''-\vec{Q}'''})}$$

$$\times\frac{1}{(\beta-E_{\vec{Q}''}-\omega_{\vec{Q}''-\vec{Q}'''}-\omega_{\vec{Q}'''-\vec{Q}'})(\beta-E_{\vec{Q}'''}-\omega_{\vec{Q}'''-\vec{Q}'})} ,$$

where $\alpha\equiv P_0-E_{\vec{Q}}$, $\beta\equiv P_0-E_{\vec{Q}'}$, and θ' is the angle between $\vec{Q}$ and $\vec{Q}'$. The above integrand is nonsingular since we work below the pion production threshold. It is convenient to take the z axis along $\vec{Q}$ and introduce a redundant integration over ϕ' ($=0$ to 2π) the azimuthal angle of $\vec{Q}'$. The resulting expression involves eight-dimensional integration, out of which five can be done analytically leaving only three for numerical integration. As in Appendix A we replace $d\Omega_{\vec{Q}',\vec{Q}}d\Omega_{\vec{Q}''',\vec{Q}}d\Omega_{\vec{Q}'',\vec{Q}}$ by $d\Omega_{\vec{Q}',\vec{Q}}d\Omega_{\vec{Q}''',\vec{Q}''}d\Omega_{\vec{Q}'',\vec{Q}}$. The special nature of the above integrand allows a further replacement of this quantity by $(2\pi)^3d\cos\psi_1d\cos\psi_2d\cos\theta''$. Here ψ_1 is the angle between $\vec{Q}''$ and $\vec{Q}'''$, and ψ_2 is the angle between $\vec{Q}'''$ and $\vec{Q}'$. Thus we get

$$\frac{g^6}{8\pi}\frac{(2\pi)^{-4}}{32P_0^2}\int\frac{(\omega_{\vec{Q}-\vec{Q}''}\omega_{\vec{Q}''-\vec{Q}'''}\omega_{\vec{Q}'''-\vec{Q}'}E_{\vec{Q}''}E_{\vec{Q}'''})^{-1}Q''^2dQ''Q'''^2dQ'''d\cos\psi_1 d\cos\psi_2 d\cos\theta''}{(\alpha-E_{\vec{Q}''}-\omega_{\vec{Q}-\vec{Q}''})(\alpha-E_{\vec{Q}'''}-\omega_{\vec{Q}-\vec{Q}''}-\omega_{\vec{Q}''-\vec{Q}'''})(P_0-E_{\vec{Q}''}-E_{\vec{Q}'''}-\omega_{\vec{Q}''-\vec{Q}'''})}$$

$$\times\frac{d\cos\theta''}{(\beta-E_{\vec{Q}''}-\omega_{\vec{Q}''-\vec{Q}'''}-\omega_{\vec{Q}'''-\vec{Q}'})(\beta-E_{\vec{Q}'''}-\omega_{\vec{Q}'''-\vec{Q}'})}\ .$$

Integrations over $d\cos\theta''$ and $d\cos\psi_2$ can be done analytically, leaving only a three-dimensional integral.

---

*Present address: Los Alamos National Laboratory, University of California, Los Alamos, NM 87545.

[1]E. E. Salpeter and H. A. Bethe, Phys. Rev. 84, 1232 (1951).

[2]In fact, the Bethe-Salpeter equation can be derived in many different ways; see N. Nakanishi, Prog. Theor. Phys. (Suppl.) 43, 1 (1969).

[3]Sometimes also called the large mass limit (static limit).

[4]R. J. Yaes, Phys. Rev. D 3, 3086 (1971).

[5]See, for example, R. Blankenbecler and R. Sugar, Phys. Rev. 142, 1051 (1966); F. Gross, *ibid.* 186, 1448 (1969); V. G. Kadyshevsky, Nucl. Phys. B6, 125 (1968); R. H. Thompson, Phys. Rev. D 1, 110 (1970); K. Erkelenz and K. Holinde, Z. Naturforsch. 28A, 353 (1973); J. M. Namyslowski, Phys. Rev. D 18, 3676 (1978).

[6]R. S. Bhalerao and S. A. Gurvitz, Phys. Rev. Lett. 47, 1815 (1981); Phys. Rev. C 24, 2773 (1981); R. S. Bhalerao, Nucl. Phys. A389, 557 (1982).

[7]S. A. Gurvitz, Weizmann Institute of Science Report No. WIS-81/47, 1981 (unpublished).

[8]In a recent paper (Ref. 9) Gross proposed a criterion to test a relativistic two-body equation. It was claimed that this criterion is satisfied by the Gross equation but not by the Bethe-Salpeter equation. For this reason he argues that the Bethe-Salpeter equation is not the "best" equation for nuclear physics, and the Gross equation is not an approximation to the Bethe-Salpeter equation. We have some reservation about this point, which we discuss in Sec. V. In this paper we therefore take the traditional viewpoint as in Refs. 10 and 11 and treat the Gross equation as a three-dimensional approximation to the Bethe-Salpeter equation.

[9]F. Gross, Phys. Rev. C 26, 2203 (1982).

[10]R. M. Woloshyn and A. D. Jackson, Nucl. Phys. B64, 269 (1973).

[11]L. Mueller and W. Gloeckle, Nucl. Phys. B146, 393 (1978).

[12]In this respect we differ from the usual rules of the old-fashioned perturbation theory; see, for example, K. Holinde, Phys. Rep. 68, 121 (1981).

[13]K. L. Kowalski, Phys. Rev. Lett. 15, 798 (1965); 15, 908(E) (1965); H. P. Noyes, *ibid.* 15, 538 (1965).

[14]This point arose during a discussion with C. M. Shakin.

[15]J. Fleischer and J. A. Tjon, Nucl. Phys. B84, 375 (1975); Phys. Rev. D 15, 2537 (1977); 21, 87 (1980); M. J. Zuilhof and J. A. Tjon, Phys. Rev. C 24, 736 (1981).

[16]M. J. Zuilhof and J. A. Tjon, Phys. Rev. C 22, 2369 (1980).